Eur. Phys. J. C (2017) 77:83
DOI 10.1140/epjc/s10052-017-4658-3

THE EUROPEAN PHYSICAL JOURNAL C

Regular Article - Experimental Physics

DAMA annual modulation and mirror Dark Matter

R. Cerulli[1], P. Villar[2,3], F. Cappella[1], R. Bernabei[4,a], P. Belli[4], A. Incicchitti[5], A. Addazi[1,6], Z. Berezhiani[1,6]

[1] INFN, Laboratori Nazionali del Gran Sasso, 67010 Assergi, AQ, Italy
[2] Laboratorio de Física Nuclear y Astropartículas, Universidad de Zaragoza, C/ Pedro Cerbuna 12, 50009 Saragossa, Spain
[3] Laboratorio Subterráneo de Canfranc, Paseo de los Ayerbe s.n., 22880 Canfranc Estación, Huesca, Spain
[4] Dipartimento di Fisica, Università di Roma "Tor Vergata" and INFN-Tor Vergata, 00133 Rome, Italy
[5] Dipartimento di Fisica, Università di Roma "La Sapienza" and INFN-Roma, 00185 Rome, Italy
[6] Dipartimento di Scienze Fisiche e Chimiche, Università di L'Aquila, 67100 Coppito, AQ, Italy

Received: 16 September 2016 / Accepted: 26 January 2017 / Published online: 8 February 2017

Abstract The DAMA experiment using ultra low background NaI(Tl) crystal scintillators has measured an annual modulation effect in the keV region which satisfies all the peculiarities of an effect induced by Dark Matter particles. In this paper we analyze this annual modulation effect in terms of mirror Dark Matter, an exact duplicate of ordinary matter from parallel hidden sector, which chemical composition is dominated by mirror helium while it can also contain significant fractions of heavier elements as Carbon and Oxygen. Dark mirror atoms are considered to interact with the target nuclei in the detector via Rutherford-like scattering induced by kinetic mixing between mirror and ordinary photons, both being massless. In the present analysis we consider various possible scenarios for the mirror matter chemical composition. For all the scenarios, the relevant ranges for the kinetic mixing parameter have been obtained taking also into account various existing uncertainties in nuclear and particle physics quantities.

1 Introduction

A peculiar annual-modulation of the counting rate is expected to be induced by Dark Matter (DM) particles in the galactic halo in a suitable set-up located deep underground on the Earth. In fact, the flux of the DM particles is modulated during the year as a consequence of the Earth revolution around the Sun which is moving in the Galactic frame [1,2]. The induced signal must satisfy simultaneously several requirements.

The DAMA Collaboration has measured an annual modulation effect over 14 independent annual cycles by using the highly radiopure NaI(Tl) detectors of the former DAMA/NaI experiment [3–32] and of the second generation DAMA/LIBRA-phase1 [33–47]. By considering the data of the 7 annual cycles collected by DAMA/NaI experiment (concluded in 2002) and of the 7 annual cycles collected by DAMA/LIBRA-phase1 an exposure of 1.33 ton × year has been released. The observed annual modulation effect points out the presence of DM particles in the Galactic halo at 9.3σ CL and the modulation amplitude of the single-hit events in the (2–6) keV energy interval is: (0.0112 ± 0.0012) cpd/kg/keV; the measured phase is (144 ± 7) days and the measured period is (0.998 ± 0.002) years, values well in agreement with those expected for DM particles [36]. No systematic effect or side reaction able to mimic the measured modulation effect, i.e. able to account for the whole measured modulation amplitude and simultaneously satisfy all of many peculiarities of the signature, was found or suggested by anyone over decades.

An important aspect of the annual-modulation measured by DAMA experiments is that this effect is model-independent. The annual modulation of the event rate is an experimental fact and it does not depend on any theoretical interpretations of the nature and interaction type(s) of DM particle signal. It can be related to a variety of interaction mechanisms of DM particles with the detector materials (see for example Ref. [40]).

The most familiar candidates for DM particles include WIMPs as lightest neutralino and axion, related respectively to well-motivated concepts of supersymmetry (+R-parity) and Peccei–Quinn symmetry which are exceptionally promising tools for solving a number of fundamental problems in particle physics. An alternative well-founded idea is that DM particles may a hidden or shadow gauge sector, with particle and interaction content similar to that of known particles. In particular, a parallel gauge sector with particle physics exactly identical to that of ordinary particles, coined as mirror world, was introduced long time ago by the reasons related to parity conservation [48–52].

[a] e-mail: rita.bernabei@roma2.infn.it

Generically, one can consider a theory based on the product $G \times G'$ of two identical gauge factors, as two copies of the Standard Model or two copies of GUTs like $SU(5) \times SU(5)$, with ordinary (O) particles belonging to a sector G and mirror (M) particles to a parallel sector G'. In General Relativity the gravity, described by the space-time metric $g_{\mu\nu}$, is the universal force equally interacting with both sectors. Therefore, the full dynamics of two sectors is governed by the Einstein–Hilbert action

$$S = \int d^4x \sqrt{-g} \left(\frac{1}{2} M_P^2 R + \mathcal{L} + \mathcal{L}' + \mathcal{L}_{\rm mix} \right), \qquad (1)$$

where M_P is the reduced Planck mass, R is the space-time curvature, the Lagrangians $\mathcal{L} = \mathcal{L}_{\rm gauge} + \mathcal{L}_{\rm Yuk} + \mathcal{L}_{\rm Higgs}$ and $\mathcal{L}' = \mathcal{L}'_{\rm gauge} + \mathcal{L}'_{\rm Yuk} + \mathcal{L}'_{\rm Higgs}$ describe the interactions in the ordinary and mirror sectors, respectively, whereas $\mathcal{L}_{\rm mix}$ describes the possible interactions between ordinary and mirror particles as e.g. photon-mirror photon kinetic mixing which shall be discussed later. The Lagrangians $\mathcal{L}$ and $\mathcal{L}'$ can be made identical by imposing mirror parity, a discrete symmetry under the exchange $G \leftrightarrow G'$ when all O particles (fermions, Higgses and gauge fields) exchange places with their M twins ('primed' fermions, Higgses and gauge fields).

Mirror matter, invisible in terms of ordinary photons but gravitationally coupled to our matter, could make a part of cosmological DM. If mirror parity is an exact symmetry, then for all ordinary particles: the electron e, proton p, neutron n, photon γ, neutrinos ν etc., with interactions described by the Standard Model $SU(3) \times SU(2) \times U(1)$, there should exist their mirror twins: e', p', n', γ', ν' etc. which are sterile to our strong, weak and electromagnetic interactions but have instead their own gauge interactions $SU(3)' \times SU(2)' \times U(1)'$ with exactly the same coupling constants. Thus, we need no new parameters for describing mirror physics: ordinary and mirror particles are degenerate in mass, and O and M sectors have identical microphysics at all levels from particle to atomic physics. In addition, the cosmological fraction of mirror baryons Ω'_B should be related to the dark baryon asymmetry as the fraction of ordinary baryons Ω_B is related to our baryon asymmetry, and baryon asymmetries in two sectors should be related to the same baryogenesis mechanism.

One could think that O and M worlds, having identical particle physics, should also have identical cosmological realisations. However, if one naively takes $\Omega'_B = \Omega_B$, then M matter is not sufficient for explaining the whole amount of DM, and other type of DM should be introduced to obtain $\Omega_{DM} \simeq 5\Omega_B$. On the other hand, if two sectors have the same temperature, $T' = T$, this would strongly disagree with the Big Bang Nucleosynthesis (BBN) limits on the effective amount of light degrees of freedom: the contribution of M particles in the universe expansion rate at the BBN epoch would be equivalent to the amount of extra neutrinos $\Delta N_{\rm eff} = 6.15$, while at most $\Delta N_{\rm eff} \simeq 0.5$ is allowed by the present constraints. In addition, due to self-interacting and dissipative nature of mirror baryons, $T' = T$ would be in full disagreement with the precision cosmological tests on the cosmic microwave background (CMB) anisotropies and the large scale structures (LSS) of the Universe, even if mirror baryons constitute a smaller fraction of cosmological DM, with $\Omega'_B = \Omega_B$.[1]

All these problems can be settled at once, if we assume that after inflation the two sectors were heated to different temperatures, and the temperature of the mirror sector T' remained less than the ordinary one T over all stages of the cosmological evolution [63]. The condition $T' < T$ can be realized by adopting the following *paradigm*: at the end of inflation the O- and M-sectors are (re)heated in an non-symmetric way, with $T > T'$, which can naturally occur in the context of certain inflationary models; the possible particle processes between O and M sectors should be slow enough and cannot bring two worlds into the equilibrium after the (re)heating, so that both systems evolve almost adiabatically and the temperature asymmetry T'/T remains nearly invariant in all subsequent epochs until the present days. In this way Mirror matter, with its atoms having the same mass as the ordinary ones, could constitute a viable candidate for asymmetric Dark Matter despite its collisional and dissipative nature.

Various potential consequences of mirror world which are worth of theoretical and experimental studies can be classified in three main parts:

A. *Cosmological implications of M baryons* The basic question is, how small the temperature ratio T'/T should be, and, on the other hand, how large the ratio Ω'_B/Ω_B between M and O baryon fractions can be, to make the concept of mirror matter cosmologically plausible. The BBN limits demand that $T'/T < 0.5$ or so, which is equivalent to $\Delta N_{\rm eff} = 0.5$ [63]. The stronger limit $T'/T < 0.3$ or so comes from cosmological considerations, by requiring the early enough decoupling of M photons which makes M baryons practically indistinguishable from the canonic Cold Dark Matter (CDM) in observational tests related to the large scale structure formation and CMB anisotropies [63–67]. The above limits apply independently whether M baryons constitute DM entirely, or only about 20% fraction of it, when $\Omega'_B \simeq \Omega_B$ [65,66]. In this case the remained 80% of DM should come from other component, presumably some sort of the CDM represented by particles belonging to the so-called WIMP class of DM candidates, by axion, or by other

[1] By these reasons, mirror matter was not considered as a serious candidate for Dark Matter for a long time, though some interesting works were done [50,51,53–55]. Also deformed asymmetric versions of mirror matter were considered, with electroweak scale larger than the ordinary one, where the atoms are heavier and more compact [56–58], and where the sterile mirror neutrinos, being much heavier than ordinary ones, could also constitute a DM fraction [59,60]. Such models have interesting implications also for the axion physics [61,62].

sort of hidden gauge sectors with heavier shadow baryons as in the case of asymmetric mirror matter [56–58], considered in our previous paper [47]. On the other hand, if DM is represented entirely by M baryons, i.e. $\Omega'_B \simeq 5\Omega_B$, then the requirement of the formation of the normal galaxies with masses larger than $10^9 M_\odot$ gives $T'/T < 0.2$ or so while the power of smaller galaxies will be suppressed by Silk damping [63,64]. Hence, cosmological evolution of the density perturbations of M matter is compatible with the observed pattern of the cosmological large scale power spectrum and the CMB anisotropies if M sector is cold enough, $T'/T < 0.2$ or so, while its collisional and dissipative nature can have specific observable implications for the evolution and formation of the structures at smaller scales, formation of galaxy halos and stars, etc. (for reviews, see e.g. [65,68,69]).

Regarding the BBN era in M sector, as far as $T' < T$, its baryonic content should be more neutron rich than in the O world since the weak interactions freeze out at higher temperatures and thus the neutron to proton ratio remains large. Hence, M sector should be helium dominated. In particular, for $T'/T < 0.3$, M world would have only 25% mass fraction of mirror hydrogen and 75% of mirror helium-4 [63], against the observed mass fractions of ordinary hydrogen (75%) and helium-4 (25%). In addition, M world can have also somewhat larger primordial metallicity than our sector. All this should have direct implications also for the formation and evolution of mirror stars [70] which produce also heavier mirror elements as oxygen, carbon etc. Future astrophysical and cosmological observations might accomplish a consistent picture of the mirror matter as Dark Matter.

Interestingly, the condition $T' < T$ have important implications also for the primordial baryogenesis, in the context of in the context of co-baryogenesis scenarios [65,71–74]. These scenarios are based B or L violating interactions which mediate the scattering processes that transform O particles into the M ones at the post-inflationary reheat epoch. Once these processes violate also CP due to complex coupling constants, while their departure from equilibrium is already implied by the condition $T' < T$, all three Sakharov's conditions can be naturally satisfied. In this way, these scenarios co-generate baryon asymmetries in both O and M sectors. Remarkably, the condition $T'/T < 0.2$ leads to a prediction $1 \leq \Omega'_B/\Omega_B \leq 5$ [65,74] which sheds a new light to the baryon and dark matter coincidence problem.

B. *Particle interactions between two sectors and oscillation phenomena* A straightforward and experimentally direct way to establish existence of mirror matter is the experimental search for oscillation phenomena between ordinary and mirror particles. In fact, any neutral particle, elementary (as e.g. neutrino) or composite (as the neutron or hydrogen atom) can mix with its mass degenerate twin from the parallel sector leading to a matter disappearance (or appearance) phenomena which can be observable in laboratories. E.g., the kinetic mixing between ordinary and mirror photons [75] induces the positronium oscillation into mirror positronium which would imitate the invisible channel of the positronium decay [76,77]. The interactions mediated by heavy gauge bosons between particles of two sectors, which can have e.g. a common flavour gauge symmetry [78] or common gauge $B-L$ symmetry [79] can induce mixing of neutral pions and Kaons with their mirror twins. The oscillation phenomena between ordinary (active) and mirror (sterile) neutrinos can have interesting observational consequences [60,80]. Interestingly, the present experimental bounds allow the neutron oscillation phenomena between two sectors to be rather fast [74], with interesting astrophysical and experimental implications [81–86]. In this respect, the relevant interaction terms between O and M particles are the ones which violate baryon B and lepton L numbers of both sectors and which can be at the origin of co-baryogenesis scenarios [65,71–74].

C. *Interaction portals and direct detection* Mirror matter can interact with ordinary matter via different portals in $\mathcal{L}_{\rm mix}$, e.g. via kinetic mixing of M and O photons, or mass mixing of M and O pions or ρ-mesons, or via contact interaction terms $\frac{1}{M}\bar{q}\gamma_\mu q\bar{q}'\gamma_\mu q'$ between O and M quarks which can be mediated by extra gauge bosons connecting two sectors [78]. In particular, there is not just one Dark Matter particle, as in most of well-motivated Dark Matter models, but it could consist of different atoms, from the primordial hydrogen and helium as dominant components, to reasonable fractions heavier elements as carbon, oxygen, etc. produced in mirror stars. The experimental direct searches of the particle DM should be concentrated on the detection of mirror helium as most abundant mirror atoms. In fact, the region of Dark Matter masses below 5 GeV is practically unexplored. In any case, for any realistic chemical composition of M sector, we know its mass spectrum of possible atomic/nuclear structures directly from our physical experience, with enormous empirical material available for ordinary atoms. Therefore, the only unknown in this puzzle is related to the interaction portal.

In this paper we mainly concentrate on this latter issue. In particular, we analyse the annual modulation observed by DAMA in the framework of mirror matter, exploiting the interaction portal related to the *photon-mirror photon kinetic mixing* term [75]

$$\frac{\epsilon}{2} F^{\mu\nu} F'_{\mu\nu} \tag{2}$$

with a small parameter $\epsilon \ll 1$. This mixing renders the mirror nuclei mini-charged with respect of ordinary electromagnetic force, and thus mediates the scattering of mirror nuclei with ordinary ones with the Rutherford-like cross sections. The implications of this detection portal was discussed in Refs. [87,88]. In our previous paper [47] we discussed it for the asymmetric mirror dark matter. In this paper we per-

form a detailed analysis of this signal in the NaI(Tl) detectors at DAMA/LIBRA set-up for exact mirror matter, for different realistic chemical compositions of mirror sector (while the dominant components should be M hydrogen and mirror helium-4, M sector can contain a mass fraction of heavier mirror atoms as Oxygen, Carbon, etc. up to few per cent), for different local temperatures and velocity flows of the mirror gas in the Galaxy.

The paper is organized as follows. In Sect. 2 we give a brief overview of mirror Dark Matter discussing its properties and possible distributions in the Galaxy. In Sect. 3 details of the analysis are given for its direct detection possibilities via photon-mirror photon kinetic mixing in the NaI(Tl) detectors of DAMA/LIBRA experiment, while in Sect. 4 we discuss the obtained results.

2 Mirror matter properties, its distribution and chemical composition in the Galaxy

How large fraction of mirror matter can be produced in baryogenesis? The baryogenesis in the two sectors, ordinary and mirror, emerges by the same mechanism, since the particle physics responsible for baryogenesis is the same in the two sectors (coupling constants, CP-violating phases, etc.). However, the cosmological conditions at the baryogenesis epoch can be different (recall that the shadow sector must be colder than the ordinary one). One can consider two cases:

1. *Separate baryogenesis*, when the baryon asymmetry in each sector is generated independently but by the same mechanism. In this case, in the most naive picture when out-of-equilibrium conditions are well satisfied in both sectors, one predicts $\eta = n_B/n_\gamma$ and $\eta' = n'_B/n'_\gamma$ must be equal, while $n'_\gamma/n_\gamma \simeq x^3 \ll 1$, where $x = T'/T$ is the temperature ratio between mirror and ordinary worlds in the early Universe. In this case, we have $\Omega'_B/\Omega_B \simeq x^3 \ll 1$. Therefore, if e.g. $x = 0.5$, a limit from BBN, we have $\Omega'_B/\Omega_B \simeq 0.15$ or so. However, one should remark that due to different out-of equilibrium conditions in the two sectors situation with $\eta' \gg \eta$ can be also obtained in some specific parameter space, where the case $\Omega'_B > \Omega_B$ can be achieved [63].
2. *Co-genesis* of baryon and mirror baryon asymmetries via $B - L$ and CP-violating processes between the ordinary and mirror particles, e.g. by the terms $\frac{1}{M} ll'HH'$ in $\mathcal{L}_{\rm mix}$ which also induce mixing between ordinary (active) and mirror (sterile) neutrinos, and which can be mediated by heavy "right-handed" neutrinos coupled to both sectors as e.g. [71–73]. In perfect out-of equilibrium conditions, when $x = T'/T \ll 1$ and so $n'_\gamma/n_\gamma \simeq x^3 \ll 1$, this leptogenesis mechanism predicts $n'_B = n_B$ and thus $\Omega'_B = \Omega_B$. In this case the cosmological fractions of ordinary and mirror baryons are equal, i.e. mirror matter can constitute only about 20% of Dark Matter in the Universe, and some other type of Dark Matter should be invoked for compelling the remaining 80%. However, if the out-of-equilibrium is not perfect, then generically final T'/T increases and one has $\Omega'_B/\Omega_B > 1$. Taking e.g. $T'/T < 0.2$, cosmological limit at which mirror matter with $\Omega'_B > \Omega_B$ is still allowed by the CMB and large scale tests, we get an upper limit $\Omega'_B/\Omega_B < 5$ or so. In this way, mirror matter could represent an entire amount of Dark Matter [65,68,69,89].

How large fraction of mirror matter can be allowed by cosmological constraints? Interestingly, for $T'/T < 0.2$, the cosmological tests (LSS and CMB) are compatible with the situation when DM is entirely represented by mirror baryons, and mirror Silk-damping allows formation of the normal size galaxies [63–66].

More difficult question is the distribution of the mirror matter in the galaxy and halo problem. At first glance M baryons, having the same physics as O matter, cannot form extended galactic halos but instead should form the disk, as usual matter does. If so, the situation with $\Omega'_B \simeq 5\Omega_B$ is excluded by observations, however $\Omega'_B \simeq \Omega_B$ remains acceptable. There should exist two disks in the Milky Way (MW), one visible and another invisible and perhaps of different radius and thickness, with comparable amount of O and M components. It is known that the total surface density of matter in the MW disk at the region of the sun is about $(68 \pm 4)\ M_\odot/\mathrm{pc}^2$ [90], while the ordinary matter can account for a fraction $(38 \pm 4) M_\odot/\mathrm{pc}^2$ or so [90]. Therefore, the surface density of mirror matter can be $(30 \pm 6) M_\odot/\mathrm{pc}^2$, perfectly compatible for the presence of dark disk similar to ours in MW. In fact, this would not contradict to the shape of the rotational velocities if the dark mirror disk is somewhat more thick than ordinary disk, and the mirror bulge is more extended than ours.

In this case, the remaining fraction of DM which should form galactic halos could come from particles belonging to the so-called WIMP class of DM candidates, from axions or from some other parallel gauge sector, like asymmetric mirror matter considered in our previous paper [47]. Interestingly, if there may be particles belonging to the so-called WIMP class of DM candidates of ordinary sector, then mirror "WIMPs" should give less contribution since M sector is colder, as well as contribution of mirror neutrinos should be smaller than that of ordinary ones [63]. Ordinary and mirror axions could give comparable contributions in DM. In any case, in what follows, we do not require that mirror baryons provide entire amount of DM, but we assume that it provides some fraction f of DM which we shall keep as an arbitrary parameter, taking $f = 0.2$ as a benchmark value.

The case whether mirror matter could be entirely Dark Matter, is difficult and it requires additional discussion. The main problem is related to galactic halos. At first glance mirror matter, having the same microphysics as ordinary matter, cannot form extended galactic halos. However, this can be possible if mirror stars are formed earlier than ordinary stars, and before the mirror matter collapsed into the disk.[2]

However, one has to take into account the possibility that in the galaxy evolution dissipative M matter, during its cooling and contraction fragments into molecular clouds in which cool rapidly and form the stars. Star formation, and moreover of the first stars, is a difficult question, however, by formal Jeans criteria, in M matter which is cooler and also helium dominated, the Jeans mass is smaller and star formation could be more efficient. In this way, mirror matter forming the stars could form, during the collapse, dark elliptical galaxies, perfectly imitating halos, while some part of survived gas could form also a dark mirror disk. In other words, we speculate on the possibility that due to faster star formation M baryons mainly form elliptical galaxies. For comparison, in MW less than one per mille of mass is contained in globular clusters and halo stars which were formed before disk formation. In MW there are up to 200 globular clusters orbiting in the Galaxy halo at distances of 50 kpc while some giant elliptical galaxies, particularly those at the centers of galaxy clusters can have as many as 10^4 globular clusters containing the overall mass $\sim 10^9 - 10^{10}\ M_\odot$. In mirror sector, if fragmentation in molecular clouds and stars is more efficient, stars are smaller and evolving faster, the elliptical galaxy can be formed by mirror stars in which ordinary matter goes mainly into disk (and also faster stellar evolution is important.) It is also possible that the mass function and chemical composition of these stars is balanced so that many of them could form black holes with masses $10-30\ M_\odot$, and among those binary black holes. This can be interesting also in view of the recent publication about gravitational wave signals from such a heavy black holes in the galaxies [94,95]. Also this can have implications for central black hole formation [63].

For Dark Matter direct detection experiments, it is important that mirror matter, being self-interacting and dissipative, cannot have the same density and velocity distributions in the Galaxy as canonical Cold Dark Matter. As far as a big fraction of mirror matter can exist in the form of mirror stars, one can rather expect that only the gas contained in the disk component is relevant for direct detection. In principle, the mirror disk can be co-rotating or counter-rotating with respect to ordinary disk, while the mirror gas at the present locality of the sun in the Galaxy can exist in the same forms that we know for the ordinary interstellar gas. Namely, it can be present in the form varying from cold molecular cloud, with temperatures $T \sim 10$ K, to warm neutral medium with $T \sim 10^4$ K and hot ionized medium with $T \sim 10^7$ K. This medium can have a local peculiar flow velocity in the galactic frame which can be dependent on the galactic coordinates and can have a value of few hundreds of km/s and certain orientation with respect to sun's velocity. In addition, in the rest frame of this medium the mirror particles will have thermal velocities which will be dependent on the particle mass. In this case the angle α between the Sun velocity and the local peculiar flow velocity can be tested by the phase of the experimental signal in a way independent on the thermal distribution velocity. In the following we consider situations with different benchmark values of the local peculiar flow velocity and of the thermal velocities. In view that mirror Dark Matter is supposed to be multi-component, consisting of not only hydrogen and helium but containing also some significant amount of heavier mirror atoms, the dependence of thermal velocity on the particle mass makes the predictions different from the CDM case when dark particles would have the same pseudo-Maxwellian velocity distribution independent on their masses.

Chemical composition of mirror matter As far as at the mirror BBN epoch the universe expansion rate is dominated by O matter density, the weak interaction's freezing in M sector occurs earlier and frozen ratio of neutrons to protons is larger than in O nucleosynthesis. As a result, primordial chemical content of M sector is helium dominated, with $^4He'$ constituting up to 80% of mass fraction of M baryons in the limit $T'/T \to 0$ [63]. In the following we take mirror helium-4 benchmark mass fraction as 75%, and mirror hydrogen as 25%. The primordial chemical content in mirror sector should also have larger metallicity that in ordinary one, but the primordial mass fraction of the heavier elements is anyway negligible.

However, heavier elements should be produced in stars and thrown in the galaxy via supernova explosions. In O sector, the chemical elements with $A \sim 16$ as Oxygen, Carbon, Nitrogen and Neon account for about a per cent of mass fraction, while heavier elements are less abundant, accounting in whole for about 4 per mille of mass fraction. In mirror sector, these proportions can be quite different. One can imagine one extreme possibility that mirror stars are typically light and do not end up as supernovae, or the gravitational collapse of heavier mirror stars typically leads to black hole formation rather than to supernova at the final stage. In this case the chemical content of mirror gas will be essentially

[2] One can consider also the possibility of the modified gravity in the context of bigravity theories [91,92] when O and M sectors have their own gravities described by two different metrics $g_{\mu\nu}$ and $g'_{\mu\nu}$, and instead of universal Hilbert–Einstein action (1), the theory is described by the action of the form $S = \int d^4x[\sqrt{-g}(\frac{1}{2}M_P^2 R + \mathcal{L}) + \sqrt{-g'}(\frac{1}{2}M_P^2 R' + \mathcal{L}') + \sqrt[4]{gg'}(\mathcal{V}_{\rm mix} + \mathcal{L}_{\rm mix})]$ where $\mathcal{V}_{\rm mix}(g^{\mu\rho}g'_{\rho\nu})$ is a mixed function of two metrics. In this situation one could have anti-gravitation phenomena between ordinary and Dark Matter at short distances and the galactic rotational curves can be well described without the need of halos, when mirror matter is entirely distributed in the disk [93].

Table 1 Abundance of elements in the Solar System

Isotope	(Z, A)	Mass fraction (in per cents)	Atom fraction (in per cents)
H	(1, 1)	70.57	91.0
He	(2, 4)	27.52	8.87
C	(6, 12)	0.30	0.032
N	(7, 14)	0.11	0.010
O	(8, 16)	0.59	0.048
Ne	(10, 20)	0.15	0.010
Si	(14, 28)	0.065	0.0030
Fe	(26, 56)	0.117	0.0027

Table 2 Typical chemical compositions of mirror matter; the mass fraction of different mirror atoms for some benchmark scenarios is reported

Mirror matter composition	H (%)	He (%)	C (%)	O (%)	Fe (%)
H′, He′	25	75	–	–	–
H′, He′, C′, O′	12.5	75.	7.	5.5	–
H′, He′, C′, O′, Fe′	20	74	0.9	5.	0.1

the same as the primordial content. i.e. dominated by helium and hydrogen. On the other extreme, one can imagine that the star formation in M sector can be more efficient, including the heavier stars with mass $>10\ M_{\odot}$. As it was studied in Ref. [70], the evolution of the latter is at least an order of magnitude faster than for ordinary heavy stars, they can produce many supernovae and so the heavier elements in M sector could be more abundant than in ordinary sector.

We assign to the mirror atoms a cosmological abundances directly rescaled from the abundances in ordinary sector (for reference, Table 1 shows the benchmark values for mass and atom fractions of different elements in the solar system). Table 2 reports typical chemical composition of mirror matter under different assumptions: (a) only primordial nuclei (H′, He′); (b) CNO elements also present; (c) also Fe′ generated by mirror supernovae explosion present.

3 Analysis

In the framework of the considered mirror model, the Dark Matter particles are expected to form, in the Galaxy, clouds and bubbles with diameter which could be even as the size of the solar system. In this modeling a dark halo, at the present epoch, is crossing a region close to the Sun with a velocity in the Galactic frame that could be, in principle, arbitrary. Hereafter we will refer to such local bubbles simply as halo. The halo can be composed by different species of mirror DM particles (different mirror atoms) that have been thermalized and in a frame at rest with the halo. They have a velocity distribution that can be considered Maxwellian with the characteristic velocity related to the temperature of the halo and to the mass of the mirror atoms. We assume that the halo has its own local equilibrium temperature, T, and the velocity parameter of the A' mirror atoms is given by $\sqrt{2k_B T/M_{A'}}$. In this scenario lighter mirror atoms have bigger velocities than the heavier ones, on the contrary of the CDM model where the velocity distribution is mass independent. If we extrapolate this assumption for electrons, in the case of hot ionized plasma with $T \sim 1$ keV, electron recoils due to elastic scattering of mirror electrons and ordinary electrons could also be relevant. In this case even some reasonable fraction of hot ionized mirror medium could give a contribution to the signal in the detector. However this contribution is model dependent since generically in the astrophysical plasma the temperature of the electrons can be different from that of the ions. Therefore, in this paper we do not concentrate on this contribution.

The expected phase of the annual modulation signal induced by the mirror particles depends on the halo velocity (module and direction) with respect to the laboratory in the Galactic frame. A detailed study on the behaviour of the annual modulation phase as a function of the halo velocity will be presented in the next section where we will show – without loosing generality – that we can consider the case of a dark halo moving either parallel or anti-parallel to the Earth in the Galactic frame.

3.1 The study of the annual modulation phase

We will use the Galactic coordinate frame, that is x axis towards the Galactic center, y axis following the rotation of the Galaxy and the z axis towards the Galactic North pole. In the following the velocity of any object can be presented as a vector $\boldsymbol{v} = (v_x, v_y, v_z)$.

The velocity of the DM particles in the laboratory frame (reference system related to the Earth) can be written as:

$$\boldsymbol{v}_{DM} = \boldsymbol{v'}_{DM} - \boldsymbol{v}_E \tag{3}$$

where $\boldsymbol{v'}_{DM}$ and $\boldsymbol{v}_E$ are the velocities of the DM particles and of the Earth in the Galactic frame, respectively. The DM particles, as described before, are enclosed inside a halo which is moving in the Galaxy with a constant velocity, $\boldsymbol{v}_{halo}$. In a frame at rest with the halo, the DM particles have a velocity, $\boldsymbol{v''}_{DM}$, that follow a Maxwellian distribution, F, depending on the assumed temperature of the system:

$$F_{A',halo}(\boldsymbol{v''}_{DM}) = \mathcal{A}\, e^{-\frac{\boldsymbol{v''}^2_{DM}}{v^2_{0,halo}}} \tag{4}$$

where $\mathcal{A}$ is a normalization constant and $v_{0,halo}$ is the velocity parameter of the distribution related to the temperature, T, of

the halo. If one considers a halo composed by mirror atoms of specie A' with $M_{A'}$ mass then $v_{0,halo} = \sqrt{2k_BT/M_{A'}}$, where k_B is the Boltzmann constant.

Since $\boldsymbol{v'}_{DM} = \boldsymbol{v''}_{DM} + \boldsymbol{v}_{halo}$, by Eq. 3 one gets:

$$\boldsymbol{v''}_{DM} = \boldsymbol{v}_{DM} + \boldsymbol{v}_E - \boldsymbol{v}_{halo} \tag{5}$$

The Earth velocity $\boldsymbol{v}_E$ in the Galactic frame can be expressed as the sum of the Sun velocity, $\boldsymbol{v}_S$, and of the revolution velocity of the Earth around the Sun, $\boldsymbol{v}_{rev}(t)$. Here we neglect the contribution of the rotation of the Earth around its axis which gives a very small effect on the annual modulation phase (it gives also rise to a diurnal modulation effect which is not of interest in this paper; see Ref. [44] for more details). Note that $\boldsymbol{v}_{rev}(t)$ depends on the sidereal time, t.

The velocity $\boldsymbol{v}_S = \boldsymbol{v}_{LSR} + \boldsymbol{v}_\odot$ can be written as the sum of the velocity of the Local Standard of Rest (LSR) due to the rotation of the Galaxy (local rotation velocity of matter in the Milky Way) $\boldsymbol{v}_{LSR} = (0, v_0, 0)$, and of the Sun peculiar velocity with respect to LSR $\boldsymbol{v}_\odot = (11.10, 12.24, 7.25)$ km/s [96,97]. The parameter v_0 is the Galactic local velocity; the estimate of v_0 ranges from (200 ± 20) km/s and (279 ± 33) km/s depending on the model of rotational curve used in its evaluation [98]. Although the interval of possible values of v_0 is rather large, in the present analysis we adopt for illustration $v_0 = (220 \pm 50)$ km/s [7,99–101] (uncertainty at 90% CL). In such a case, one has $|\boldsymbol{v}_S| = (232 \pm 50)$ km/s.

Hence, the velocity distribution of the DM particles (A' mirror atoms) in the laboratory frame becomes:

$$F_{A'}(\boldsymbol{v}_{DM}) = \mathcal{A}\, e^{-\frac{(\boldsymbol{v}_{DM}+\boldsymbol{v}_E-\boldsymbol{v}_{halo})^2}{v^2_{0,halo}}} \tag{6}$$

The annual modulation of the counting rate and its phase depend on the relative velocity distribution of the DM particles with respect to the laboratory frame (Eq. 6). Thus, once averaging over the angles, they depend on the module of $\boldsymbol{v}_{rel}(t) = \boldsymbol{v}_E - \boldsymbol{v}_{halo}$. Since $|\boldsymbol{v}_{rel}(t)|$ depends on the time revolution of the Earth around the Sun, the counting rate shows the typical modulation behaviour: $\mathcal{S}(t) = \mathcal{S}_0 + \mathcal{S}_m cos\omega(t - t_0)$ where t_0 is the phase of the annual modulation and $T_p = 2\pi/\omega = 1$ sidereal year is the period.

In the following we calculate the expected phase t_0 as a function of the halo velocity.

The motion of the Earth around the Sun can be worked out by using the ecliptic coordinate system $(\hat{e}_1^{ecl}, \hat{e}_2^{ecl}, \hat{e}_3^{ecl})$, where the $\hat{e}_1^{ecl}$ axis is directed towards the vernal equinox and $\hat{e}_1^{ecl}$ and $\hat{e}_2^{ecl}$ lie on the ecliptic plane. The right-handed convention is used. In the Galactic coordinates, we can write (see Ref. [44] for details):

$$\begin{aligned}
\hat{e}_1^{ecl} &= (-0.05487, 0.49411, -0.86767),\\
\hat{e}_2^{ecl} &= (-0.99382, -0.11100, -0.00035),\\
\hat{e}_3^{ecl} &= (-0.09648, 0.86228, 0.49715).
\end{aligned} \tag{7}$$

The ecliptic plane is tilted with respect to the galactic plane by $\approx 60°$, as $\hat{e}_3^{ecl} \cdot (0, 0, 1) = 0.49715$. So the evolution of the Earth in the ecliptic plane can be described as:

$$\boldsymbol{v}_{rev}(t) = v_{ov}\,(\hat{e}_1^{ecl} \sin\lambda(t) - \hat{e}_2^{ecl} \cos\lambda(t)) \tag{8}$$

where v_{ov} is the orbital velocity of the Earth which has a weak dependence on time due to the ellipticity of the Earth orbital motion around the Sun. Its value ranges between 29.3 and 30.3 km/s; for most purposes it can be assumed constant and equal to its mean value $\simeq$29.8 km/s. On the other hand, when more accurate calculations are necessary, the routines in Ref. [102] can be used: they also take into account the ellipticity of the Earth orbit and the gravitational influence of other celestial bodies (Moon, Jupiter, and etc.) Moreover, the phase in Eq. 8 can be written as $\lambda(t) = \omega(t - t_{equinox})$, where t is the sidereal time and $t_{equinox}$ is the spring equinox time ($\approx$March 21).

The time-independent part of $\boldsymbol{v}_{rel}(t)$ is given by $\boldsymbol{v}_{ti} = \boldsymbol{v}_{LSR} + \boldsymbol{v}_\odot - \boldsymbol{v}_{halo}$, while the time-dependent one is $\boldsymbol{v}_{rev}(t)$. Thus:

$$|\boldsymbol{v}_{rel}(t)| = \sqrt{v_{ti}^2 + v_{ov}^2 + 2\,\boldsymbol{v}_{ti} \cdot \boldsymbol{v}_{rev}(t)} \tag{9}$$

The scalar product in the previous equation can be written as:

$$\boldsymbol{v}_{ti} \cdot \boldsymbol{v}_{rev}(t) = v_{ov}(\boldsymbol{v}_{ti} \cdot \hat{e}_1^{ecl} \sin\lambda(t) - \boldsymbol{v}_{ti} \cdot \hat{e}_2^{ecl} \cos\lambda(t)). \tag{10}$$

Defining $\hat{v}_{ti} \cdot \hat{e}_1^{ecl} = A_m \sin\beta_m$ and $-\hat{v}_{ti} \cdot \hat{e}_2^{ecl} = A_m \cos\beta_m$ which depend on the assumed DM halo velocity in the Galaxy $\boldsymbol{v}_{halo}$, Eq. 10 becomes:

$$\begin{aligned}
\boldsymbol{v}_{ti} \cdot \boldsymbol{v}_{rev}(t) &= v_{ov}\, v_{ti}\, A_m \cos(\lambda(t) - \beta_m)\\
&= v_{ov}\, v_{ti}\, A_m \cos\omega(t - t_0).
\end{aligned} \tag{11}$$

A_m and β_m can be calculated once the halo velocity and the v_0 value are fixed. Then, substituting the Eq. 11 in Eq. 9, one gets:

$$|\boldsymbol{v}_{rel}(t)| = v_{med}\,\sqrt{1 + 2\delta\,\cos\omega(t - t_0)} \tag{12}$$

where

$$\delta = \frac{v_{ov}\, v_{ti}\, A_m}{v_{ti}^2 + v_{ov}^2}. \tag{13}$$

and $v_{med} = \sqrt{v_{ti}^2 + v_{ov}^2}$.

For those values of $\boldsymbol{v}_{halo}$ so that $v_{ti} \gg v_{ov} \simeq 30$ km/s, one gets $\delta \ll 1$, and:

$$|\boldsymbol{v}_{rel}(t)| \simeq v_{med}\,(1 + \delta\,\cos\omega(t - t_0)) \tag{14}$$

that is the usual case of a DM halo at rest in the Galactic frame.

In the general case the phase of the DM annual modulation is determined at the time when the argument of the cosine in Eq. 12 is null:

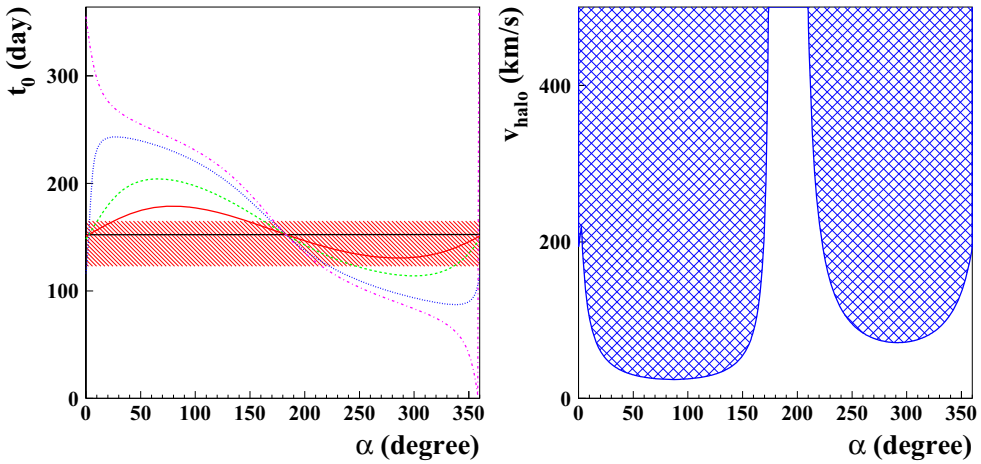

Fig. 1 *Left* Examples of expected phase of the annual modulation signal as a function of the angle, α, between the Sun velocity and the velocity of the DM mirror halo moving in the Galactic plane. The different curves refer to different values of the module of the halo velocity: 300 km/s (*dashed-dotted*), 200 km/s (*dotted*), 100 km/s (*dashed*), 50 km/s (*solid*). The *shaded area* (*red on-line*) is defined by the values of the phase of the annual modulation signal allowed at 3σ by DAMA. For each halo velocity, only the values of α included inside the *shaded area* are allowed. The *solid horizontal black line* corresponds to a halo at rest in the Galactic frame ($\boldsymbol{v}_{halo} = 0$) giving a phase equal to 152.5 day (June 2nd). *Right* The *shaded regions* in the plane v_{halo} *vs* α correspond to halo velocities (module and direction) giving a phase that differs more than 3σ from the phase of the annual modulation effect measured by DAMA. These velocities in the shaded regions are thus excluded by the DAMA results at 3σ CL

$$t_0 = t_{equinox} + \beta_m/\omega, \tag{15}$$

and $|\boldsymbol{v}_{rel}(t)|$ assumes its maximal value.

In conclusion, the annual modulation phase depends on the module of the halo velocity (i) and on the relative direction of the halo with respect to the Earth velocity (ii). The case of a mirror DM halo with a null velocity corresponds to the description generally considered for the DM halo in which it is at rest in the Galactic frame; in particular, in this case the expected phase of the annual modulation is around June 2nd.

In the present analysis we are interested only in scenarios compatible with the annual modulation phase measured experimentally by DAMA. We recall that, considering the annual cycles collected with DAMA/NaI and the annual cycles of DAMA/LIBRA-phase1, the best fit value of the phase obtained by the measured residual rate in 2–6 keV energy range is 144 ± 7 days [36].

The curves in Fig. 1-*left* show, as examples for halos moving in the galactic plane, the expected phase of the annual modulation signal as a function of the angle, α, between the Sun velocity and the halo velocity: $\cos\alpha = \hat{v}_S \cdot \hat{v}_{halo}$; they have been obtained for four different values of the halo velocity module.

As it can be easily inferred, when the halo velocity is anti-parallel to the Sun velocity ($\alpha \simeq \pi$) the phase of the annual modulation is $\simeq$June 2nd for any module of $\boldsymbol{v}_{halo}$. For parallel halo velocity ($\alpha \simeq 0$) depending whether or not v_{halo} is larger than v_S the phase of annual modulation can be even reversed. The 3σ region compatible with the DAMA annual modulation phase is also reported as shaded area (red on-line); the points included inside the shaded area are allowed by the DAMA result. The solid horizontal black line corresponds to a halo at rest in the Galactic frame ($\boldsymbol{v}_{halo} = 0$) giving a phase equal to 152.5 day (June 2nd).

The module of the halo velocity that corresponds to a phase compatible at 3σ CL with the annual modulation phase measured by DAMA can be worked out for each α value. The result is reported in Fig. 1-*right* where the configurations giving a phase that exceed by 3σ from the one measured by DAMA are shaded in the plot.

Finally, in Fig. 2 the directions of the halo velocity in Galactic Coordinate compatible with the DAMA annual modulation phase are reported for four different values of the velocity module.

The results shows that many scenarios exist that are compatible with the annual modulation observed by DAMA. Without losing generality, in the rest of the paper we will consider only halo velocities parallel or anti-parallel to the Sun ($\alpha \simeq 0$ and $\simeq \pi$, respectively). For these configurations (for $\alpha \simeq 0$ when $v_{halo} < v_S$) the expected phase is $\simeq$June 2nd, as in the case of a halo at rest with respect to the Galactic Center. The only parameter whose value will be varied in the analysis is the module of the velocity. For convention positive velocity will correspond to halo moving in the same direction of the Sun while negative velocity will correspond to opposite direction.

3.2 Interaction rates

The low-energy differential cross-section of the scattering between the ordinary and mirror atoms is essentially the same

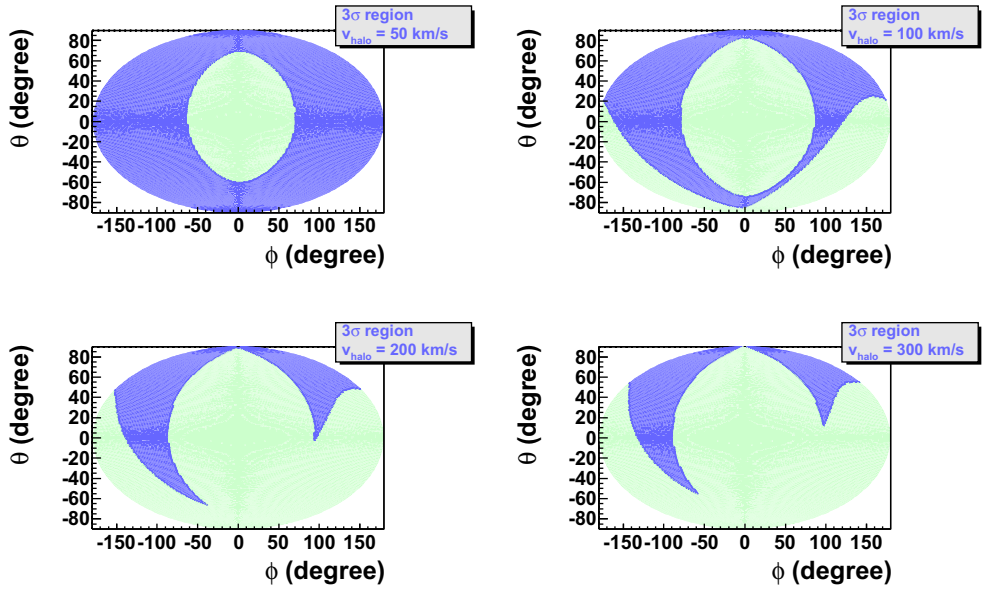

Fig. 2 The *dark* (*blue on-line*) regions correspond to directions of the halo velocities in Galactic Coordinate (θ, ϕ) giving a phase compatible at 3σ CL with the annual modulation phase measured by DAMA. The four panels refer to different values of the velocity module: 50, 100, 200, 300 km/s

as the cross section $\mathcal{N}' + \mathcal{N} \to \mathcal{N}' + \mathcal{N}$ between the respective nuclei, mirror $\mathcal{N}'$ with a mass M'_A and mirror electric charge Z' and an ordinary $\mathcal{N}$ with a mass M_A and an electric charge Z, mediated by the photon – mirror photon kinetic mixing; it has the Rutherford-like form [87]:

$$\frac{d\sigma_{A,A'}}{dE_R} = \frac{\mathcal{C}_{A,A'}}{E_R^2 v_{DM}^2}, \tag{16}$$

where E_R is the recoil energy of the ordinary nucleus, v_{DM} is the relative velocity between the nuclei $\mathcal{N}'$ and $\mathcal{N}$, and

$$\mathcal{C}_{A,A'} = \frac{2\pi\epsilon^2\alpha^2 Z^2 Z'^2}{M_A}\mathcal{F}_A^2\mathcal{F}_{A'}^2, \tag{17}$$

where α is the fine structure constant, and $\mathcal{F}_X(qr_X)$ $(X = A, A')$ are the Form-factors of ordinary and mirror nuclei, which depend on the momentum transfer, q, and on the radius of X nucleus. The effect of the e' screening will be negligible since the mirror atoms are not compact, i.e. the inverse radius of the mirror atom $1/a' \simeq \alpha m_e$ is smaller than the transfer momentum $q = \sqrt{2M_A E_R}$. In particular, for Na target in DAMA, considering that the relevant recoil energy range is 2–6 keV electron equivalent which corresponds to $E_R \simeq 6-20$ keV when one takes into account a quenching factor value around 0.3 we have $q > 20$ MeV, so that the condition $1/q < a'$ is fully satisfied.

The differential interaction rate of mirror nuclei of different species on a target composed by more than one kind of nucleus is:

$$\begin{aligned}\frac{d\mathcal{R}}{dE_R} &= \sum_{A,A'} N_A \chi_{A'} \int \frac{d\sigma_{A,A'}}{dE_R} F_{A'}(\boldsymbol{v}_{DM}) v_{DM} d^3 v_{DM} \\ &= \sum_{A,A'} N_A \chi_{A'} \frac{\mathcal{C}_{A,A'}}{E_R^2} \int_{v_{DM} > v_{min}(E_R)} \frac{F_{A'}(\boldsymbol{v}_{DM})}{v_{DM}} d^3 v_{DM},\end{aligned} \tag{18}$$

where: (i) N_A is the number of the target atoms of specie A per kg of detector; (ii) $\chi_{A'} = \rho_{DM}\Upsilon_{A'}/M_{A'}$ with ρ_{DM} halo mirror matter density, $\Upsilon_{A'}$ fraction of the specie A' in the dark halo, and $M_{A'}$ mass of the mirror nucleus A'; (iii) the sum is performed over the mirror nuclei involved in the interactions (A') and over the target nuclei in the detector (A). We can normalize ρ_{DM} to a reference value $\rho_0 = 0.3$ GeV/cm^3 as $\rho_{DM} = f\,\rho_0$; thus all numerical results presented below will be written in terms of $\sqrt{f}\epsilon$.

The lower velocity limit $v_{min}(E_R)$ is

$$v_{min}(E_R) = \sqrt{\frac{(M_A + M_{A'})^2 E_R}{2M_A M_{A'}^2}}. \tag{19}$$

The theoretical differential counting rate can be written as:

$$\frac{d\mathcal{R}}{dE} = \sum_A \int \mathcal{K}_{\mathcal{A}}(E|E_R)\frac{d\mathcal{R}_{\mathcal{A}}}{dE_R} dE_R, \tag{20}$$

where $\frac{d\mathcal{R}_{\mathcal{A}}}{dE_R}$ is the differential interaction rate on the A nucleus in the detector. The $\mathcal{K}_{\mathcal{A}}(E|E_R)$ kernel can be written as [47]:

$$\mathcal{K}_{\mathcal{A}}(E|E_R) = \int \mathcal{G}(E|E')\mathcal{Q}_{\mathcal{A}}(E'|E_R) dE', \tag{21}$$

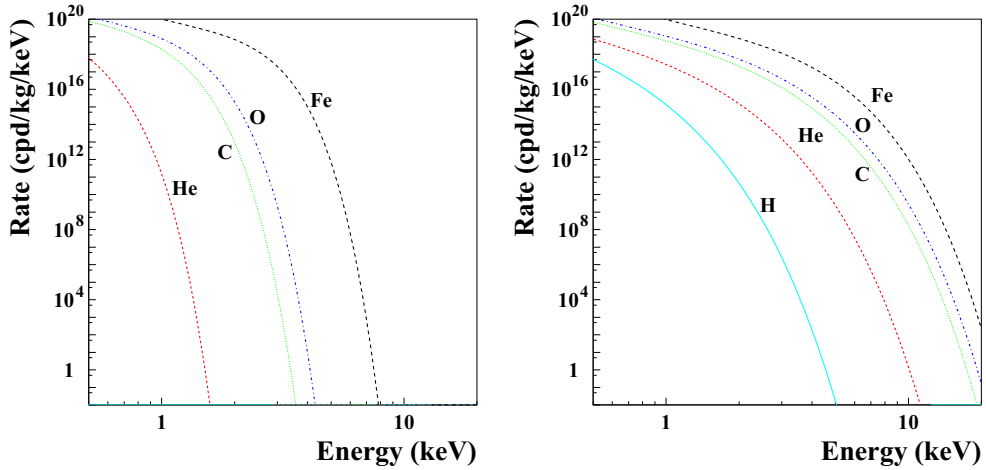

Fig. 3 Constant part of the annual modulation signal expected for only one mirror atom specie in a NaI(Tl) detector, by considering $\sqrt{f}\epsilon = 1$. Few different mirror atoms are reported. The two panels refer to the case of cold ($T = 10^4$ K) (*left panel*) and hot ($T = 10^7$ K) (*right panel*) halo with $v_{halo} = 100$ km/s. The considered scenario is the case *a* of Table 3 in set A (see Sect. 4.4)

where $\mathcal{G}(E|E')$ takes into account the energy resolution of the detector, while $\mathcal{Q}_{\mathcal{A}}(E'|E_R)$ takes into account the energy transformation of the nuclear recoil energy in keV electron equivalent (hereafter indicated simply as keV) through the quenching factor (see later). For example, the latter kernel can be written in the simplest case of a constant quenching factor q_A as: $\mathcal{Q}_{\mathcal{A}}(E'|E_R) = \delta(E' - q_A E_R)$.

Defining $\eta(t) = v_{rel}(t)/v_0$, when the Eq. 14 holds, one gets: $\eta(t) = \eta_0 + \Delta\eta cos\omega(t - t_0)$, where η_0 is the yearly average of η and $\Delta\eta$ is its maximal variation along the year. Since, in this case, $\Delta\eta \ll \eta_0$, the expected counting rate can be expressed by the first order Taylor expansion:

$$\frac{d\mathcal{R}}{dE}[\eta(t)] = \frac{d\mathcal{R}}{dE}[\eta_0] + \frac{\partial}{\partial\eta}\left(\frac{d\mathcal{R}}{dE}\right)_{\eta=\eta_0} \Delta\eta\cos\omega(t - t_0). \tag{22}$$

Averaging this expression in a given energy interval one obtains:

$$\begin{aligned}\mathcal{S}[\eta(t)] &= \mathcal{S}[\eta_0] + \left[\frac{\partial\mathcal{S}}{\partial\eta}\right]_{\eta_0} \Delta\eta cos\omega(t - t_0) \\ &= \mathcal{S}_0 + \mathcal{S}_m cos\omega(t - t_0),\end{aligned} \tag{23}$$

with the contribution from the higher order terms less than 0.1%; $\mathcal{S}_m$ and $\mathcal{S}_0$ are the modulated and the unmodulated part of the expected differential counting rate, respectively.

The cross-section (Eq. 16) strongly depends on the kinetic mixing parameter ϵ. On the other hand, there are direct experimental limits on it from the ortopositronium oscillation into mirror ortopositronium [76,77]. The latest limit on the experimental search reads $\epsilon < 4 \times 10^{-7}$ [103]. The cosmological limits are more stringent, from the condition that $e^+e^- \to e'^+e'^-$ process mediated by this kinetic mixing will not heat too much the mirror bath [104]. Namely, the condition $T'/T < 0.3$ implies $\epsilon < 3 \times 10^{-9}$ or so [105]. As we see below, our results for Dark Matter detection are compatible with the existing limits on the Dark Matter particle mini-charges, or in some situation in some tension with the cosmological limit.[3]

In Fig. 3 the behaviour of the unmodulated part of the signal expected for only one mirror atom specie in a NaI(Tl) detector in a template case is reported. In this Fig. $\sqrt{f}\epsilon = 1$, few mirror atoms and two different halo temperatures have been considered.

4 Details of the analysis

The data analysis in the symmetric mirror DM model considered here allows the determination of the $\sqrt{f}\epsilon$ parameter. As mentioned this corollary analysis is model dependent. The main aspects which enter in the $\sqrt{f}\epsilon$ determination and the related uncertainties are pointed out in Ref. [47]. Here we just remind few items.

4.1 Phase-space distribution functions of DM mirror particles in the dark halo

Mirror dark halo is composed by dark atoms of different species having Maxwellian velocity distribution in a frame where the halo is at rest. The halo has its own equilib-

[3] In principle, the parameter ϵ can be a dynamical degree of freedom which varied during the evolution of the universe [106]. Thus, one cannot exclude the situation that $\epsilon \sim 10^{-7}$ today but it was $<10^{-9}$ at the BBN epoch, and thus one take as a limit direct experimental bound $\epsilon < 4 \times 10^{-7}$ [103]. It is interesting that for larger values of ϵ, the electron drag due to relative rotation of ordinary and mirror plasma components during the galaxy formation can give rise to circular electric currents which can originate galactic magnetic fields [107].

rium temperature T and the velocity parameter of the A' mirror atoms is given by $\sqrt{2k_BT/M_{A'}}$. In the analysis we have considered different temperature regimes: cold halo ($T \simeq 10^4-10^5$ K) and hot halo ($T \gtrsim 10^6-10^8$ K). For simplicity the escape velocity of mirror atoms in the halo has been considered infinite.

4.2 Nuclei and Dark Matter form factors

As regard the nuclei and DM form factors, entering in the determination of the expected signal counting rate, a *Helm form factor* [108,109] has been considered[4] for each X ordinary and mirror nucleus. Details on the used form factors can also be found in Ref. [47]. In the analysis some uncertainties on the nuclear radius and on the nuclear surface thickness parameters in the Helm SI form factors have been included (see e.g. [14,37]).

4.3 Quenching factors and channeling effect

Following the procedure reported in Refs. [21,37,47], in the present analysis three possibilities for the Na and I quenching factors have been considered: (Q_I) the quenching factors of Na and I "constants" with respect to the recoil energy E_R: $q_{Na} \simeq 0.3$ and $q_I \simeq 0.09$ as measured by DAMA with neutron source integrated over the $6.5-97$ keV and the $22-330$ keV recoil energy range, respectively [4]; (Q_{II}) the quenching factors evaluated as in Ref. [110] varying as a function of E_R; (Q_{III}) the quenching factors with the same behaviour of Ref. [110], but normalized in order to have their mean values consistent with Q_I in the energy range considered there.

A detailed discussion about the uncertainties in the quenching factors has been given in section II of Ref. [37] and in Ref. [47]. In fact, the related uncertainties affect all the results both in terms of exclusion plots and in terms of allowed regions/volumes; thus, comparisons with a fixed set of assumptions and parameters values are intrinsically strongly uncertain.

Another important effect is the *channeling* of low energy ions along axes and planes of the NaI(Tl) DAMA crystals. This effect can lead to an important deviation, in addition to the other uncertainties discussed in section II of Ref. [37] and in Ref. [47]. In fact, the *channeling* effect in crystals implies that a fraction of nuclear recoils are channeled and experience much larger quenching factors than those derived from neutron calibration (see [19,37] for a discussion of these aspects). The channeling effect in solid crystal detectors is not a well fixed issue. There are a lot of uncertainties in the modeling. Moreover, the experimental approaches (as that in Ref. [111]) are rather difficult since the channelled nuclear recoils are – even in the most optimistic model – a very tiny fraction of the not-channeled recoils. In particular, the modeling of the *channeling* effect described by DAMA in Ref. [19] is able to reproduce the recoil spectrum measured at neutron beam by some other groups (see Ref. [19] for details). For completeness, we mention the alternative *channeling* model of Ref. [112], where larger probabilities of the planar channeling are expected, and the analytic calculation where the *channeling* effect holds for recoils coming from outside a crystal and not from recoils from lattice sites, due to the blocking effect [113]. Nevertheless, although some amount of blocking effect could be present, the precise description of the crystal lattice with dopant and trace contaminants is quite difficult and analytical calculations require some simplifications which can affect the result. Because of the difficulties of experimental measurements and of theoretical estimate of the *channeling* effect, in the following it will be either included using the procedure given in Ref. [19] or not in order to give idea on the related uncertainty.

4.4 Further uncertainties

In case of low mass DM particles giving rise to nuclear recoils it is also necessary to account for the Migdal effect. A detailed discussion of its impact in the corollary analyses in terms of some DM candidates is given in Refs. [18,47].

Moreover, to take into account the uncertainty on the local velocity, v_0, following the discussion in Sect. 3.1 we have considered the discrete values: 170, 220 and 270 km/s.

Finally, some discrete cases are considered to account for the uncertainties on the measured quenching factors and on the parameters used in the nuclear form factors, as already done in previous analyses for other DM candidates and scenarios. The first case (set A) considers the mean values of the parameters of the used nuclear form factors [14] and of the quenching factors. The set B adopts the same procedure as in Refs. [9,10], by varying (i) the mean values of the ^{23}Na and ^{127}I quenching factors as measured in Ref. [4] up to $+2$ times the errors; (ii) the nuclear radius, r_A, and the nuclear surface thickness parameter, s, in the form factor from their central values down to -20%. In the last case (set C) the Iodine nucleus parameters are fixed at the values of case B, while for the Sodium nucleus one considers: (i) ^{23}Na quenching factor at the lowest value measured in literature; (ii) the nuclear radius, r_A, and the nuclear surface thickness parameter, s, in the SI form factor from their central values up to $+20\%$.

[4] It should be noted that the Helm form factor is the less favorable one e.g. for iodine and requires larger SI cross-sections for a given signal rate; in case other form factor profiles, considered in the literature, would be used [14], the allowed parameters space would extend.

4.5 Analysis procedures

The analysis procedure has been described in Ref. [47]. Here we just remind that the obtained χ^2 for the considered mirror DM model is function of only one parameter: $\sqrt{f}\epsilon$; thus, we can define:

$$\Delta\chi^2\{\sqrt{f}\epsilon\} = \chi^2\{\sqrt{f}\epsilon\} - \chi^2\{\sqrt{f}\epsilon = 0\}.$$

The $\Delta\chi^2$ is a χ^2 with one degree of freedom and is used to determine the allowed interval of the $\sqrt{f}\epsilon$ parameter at 5σ from the *null signal hypothesis*.

5 Results

In the data analysis we have taken into account all the uncertainties discussed in the previous sections. The scenarios summarized in Table 3 have been considered depending on: (i) the adopted quenching factors; (ii) either inclusion or not of the channeling effect; (iii) either inclusion or not of the Migdal effect. For each scenario the different halo compositions reported in Table 2 have been considered, with halo temperature in the range 10^4-10^8 K and with halo velocity from -400 to $+300$ km/s. The uncertainties, described in the three sets given in Sect. 4.4, have been considered.

Table 3 Summary of the scenarios considered in the present analysis of the DAMA data in terms of mirror DM framework as discussed in the text

Scenario	Quenching factor	Channeling	Migdal
a	Q_I [4]	No	No
b	Q_I [4]	Yes	No
c	Q_I [4]	No	Yes
d	Q_{II} [110]	No	No
e	Q_{III} [110]-normalized	No	No

Firstly we show in Fig. 4 the behaviour of the modulated part, S_m of the Dark Matter signal obtained by fitting the considered DM mirror model with the DAMA annual modulation data. Two composite halo models (left: H′(12.5%), He′(75%), C′(7%), O′(5.5%), right: H′(20%), He′(74%), C′(0.9%), O′(5%), Fe′(0.1%)) having different temperatures in different frameworks have been considered as examples. The contribution to the signal coming from each mirror atom species are reported. In both case the most relevant contribution comes from the O′ dark atoms while the contribution of the H′ is negligible. It is interesting to note that the profile of the modulated signal below 2 keV is different for the two halo models; this can be studied by DAMA/LIBRA, now running in its phase2 with a software energy threshold down to 1 keV.

In the following, we present the $\sqrt{f}\epsilon$ values allowed by DAMA in different halo modeling and various scenarios. In particular, we present two different plots for each halo composition. We report: (i) allowed regions for the $\sqrt{f}\epsilon$ parameter as a function of the halo temperature for different values of the halo velocity in the Galactic frame; (ii) allowed regions for the $\sqrt{f}\epsilon$ parameter as a function of the halo velocity in the Galactic frame for different halo temperature. All the allowed intervals reported identify the $\sqrt{f}\epsilon$ values corresponding to CL larger than 5σ from the *null hypothesis*, that is $\sqrt{f}\epsilon = 0$.

In Fig. 5 for template purpose only the case set A and $v_0 = 220$ km/s is depicted considering a halo composed only by He' dark atoms. The cases of halos made either only of O', or only of C' or only of Fe' are reported in Figs. 6, 7 and 8, respectively.

The result corresponding to composite halos are reported in Fig. 9, in Fig. 10 and in Fig. 11 where the cases: (i) H′(24%), He′(75%), Fe′(1%); (ii) H′(20%), He′(74%), C′(0.9%), O′(5%), Fe′(0.1%), (iii) H′(12.5%), He′(75%), C′(7%), O′(5.5%), have been considered respectively. In par-

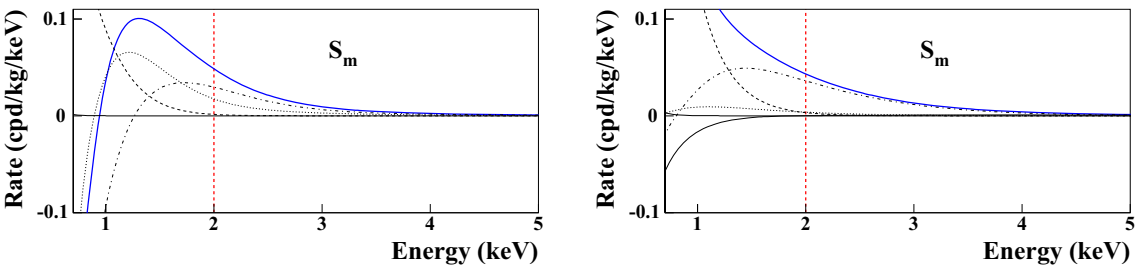

Fig. 4 Examples of expected modulation amplitude, S_m, of the DM signal for the mirror DM candidates in the scenario (*b*) (*left*) and (*a*) (*right*) of Table 3, for two different halo compositions. *Left* Composite dark halo: H′(12.5%), He′(75%), C′(7%), O′(5.5%), with halo velocity $v_{halo} = 30$ km/s, temperature $T = 10^6$ K, $v_0 = 220$ km/s and parameters in the set A. The contributions to the signal (*solid line*, *blue on-line*) of the different dark atoms are depicted: H′ (not visible), He′ (*dashed*), C′ (*dotted*), O' (*dashed-dotted*). *Right* Composite dark halo: H′(20%), He′(74%), C′(0.9%), O′(5%), Fe′(0.1%), with halo velocity $v_{halo} = 0$ km/s, temperature $T = 10^7$ K, $v_0 = 220$ km/s and parameters in the set A. The contributions to the signal (*solid line*, *blue on-line*) due to the different dark atoms are depicted: H′ (*solid line*, visible well below 1 keV), He′ (*dashed*), C′ (*dotted*), O′ (*dashed-dotted*), Fe′ (*solid* and negative below 2 keV)

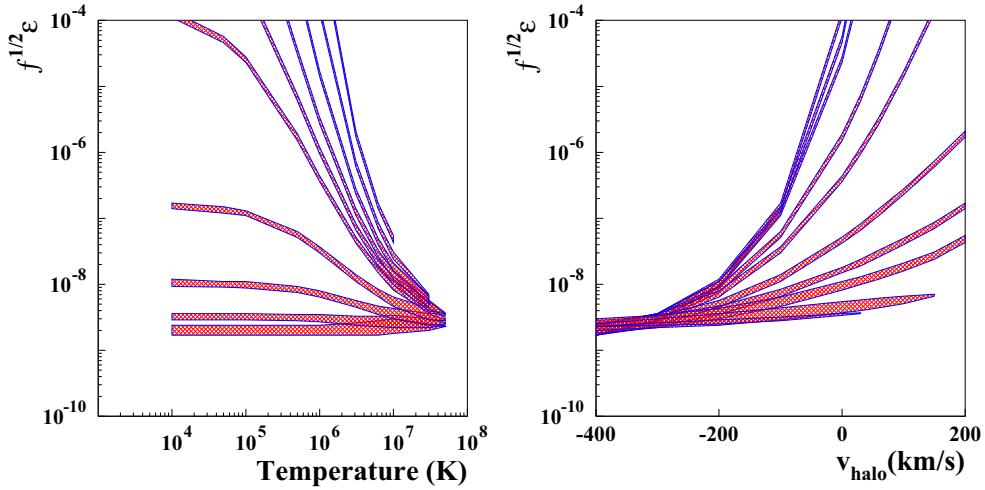

Fig. 5 Case of halo composed by pure He' dark atoms in the scenario (*a*) of Table 3 with $v_0 = 220$ km/s and parameters in the set A (see text). *Left* Allowed regions for the $\sqrt{f}\epsilon$ parameter as a function of the halo temperature for different values of the halo velocity in the Galactic frame: $-400, -300, -200, -100, 0, 30, 60, 100, 150, 200$ km/s. Increasing the halo velocity the allowed regions e.g. at temperature of 10^4 K move to higher values of $\sqrt{f}\epsilon$ parameter. *Right* Allowed regions for the $\sqrt{f}\epsilon$ parameter as function of the halo velocity in the Galactic frame for different halo temperature: $10^4, 5 \times 10^4, 10^5, 5 \times 10^5, 10^6, 3.1 \times 10^6, 6.2 \times 10^6, 10^7, 3 \times 10^7, 5 \times 10^7$ K Increasing the temperature the allowed region at large positive v_{halo} move to small values of $\sqrt{f}\epsilon$ parameter. These allowed intervals identify the $\sqrt{f}\epsilon$ values corresponding to CL larger than 5σ from the null annual modulation hypothesis, that is $\sqrt{f}\epsilon = 0$

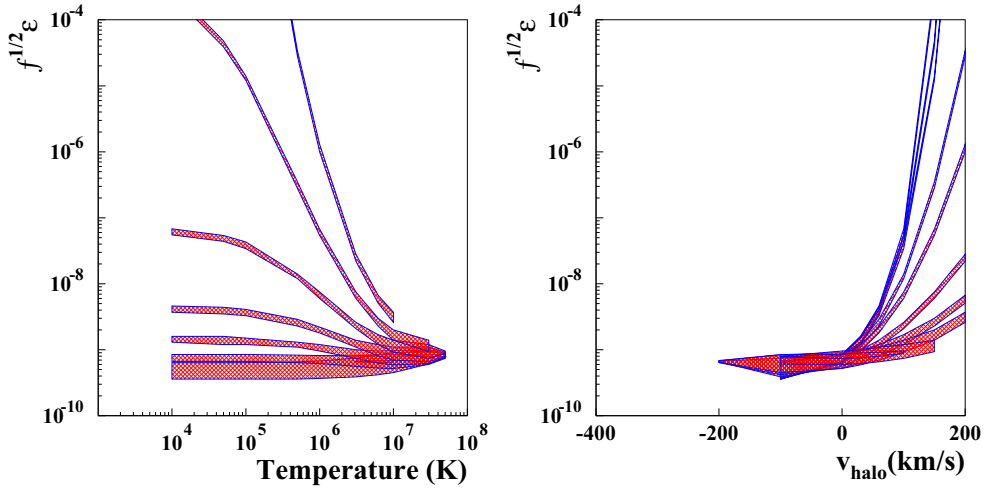

Fig. 6 Case of halo composed just by pure C' dark atoms in the scenario (*a*) of Table 3 with $v_0 = 220$ km/s and parameters in the set A (see text and Fig. 5). The different values of the halo velocity in the *left plot* are: $-200, -100, 0, 30, 60, 100, 150, 200$ km/s. The different values of the halo temperature in the *right plot* are as those of Fig. 5

ticular, in the case (i) we introduce 1% of Fe′ for demonstrating how much heavier nuclei can influence the signal.

As it can be expected, considering for example the behaviour of unmodulated part of the dark atom signal depicted in Fig. 3, the allowed regions – in all the considered scenarios – move toward lower value of $\sqrt{f}\epsilon$ parameter when the dark atoms of the halo are heavier with higher charge numbers; in this case the interaction cross section increases and, in order to keep the same strength of the DM signal, lower value of coupling are preferred. The lowest allowed regions is obtained for a pure Fe' halo. For each scenario there are two regimes: for cold halo the allowed $\sqrt{f}\epsilon$ parameter increases with the halo velocity while the parameter converges to a lower value for hot halo regardless its velocity in the Galactic frame. In cold scenario the dark atoms kinetic energy in the halo is small and the relative velocity of the halo with respect to the Earth is the dominant contribution to the average velocity of the particles in

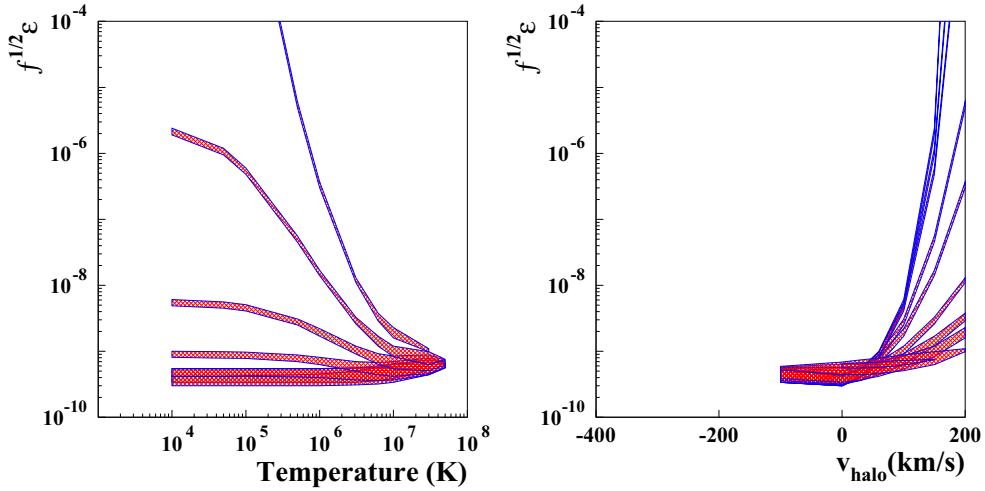

Fig. 7 Case of halo composed just by pure O' dark atoms in the scenario (a) of Table 3 with $v_0 = 220$ km/s and parameters in the set A (see text and Fig. 5). The different values of the halo velocity in the left plot are: -100, 0, 30, 60, 100, 150, 200 km/s. The different values of the halo temperature in the right plot are as those of Fig. 5

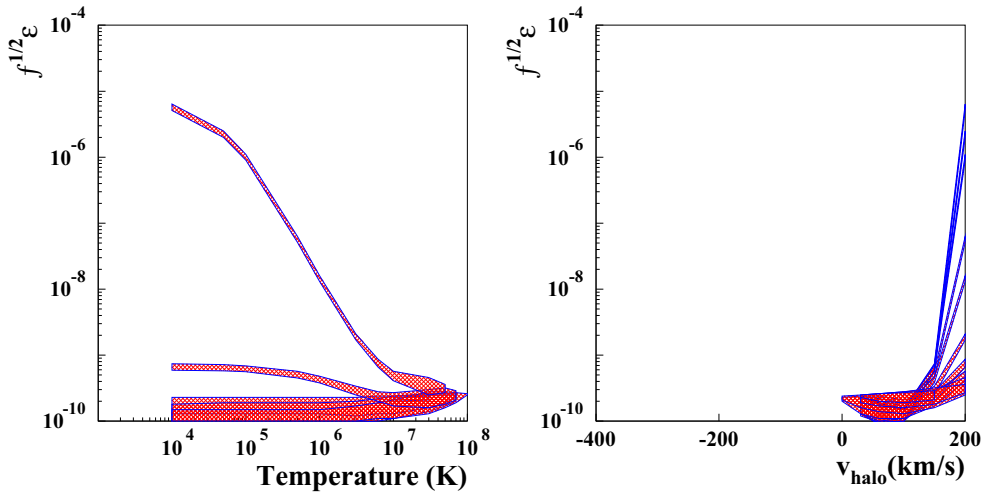

Fig. 8 Case of halo composed just by pure Fe' dark atoms in the scenario (a) of Table 3 with $v_0 = 220$ km/s and parameters in the set A (see text and Fig. 5). The different values of the halo velocity in the left plot are: 0, 30, 60, 100, 150, 200 km/s. The different values of the halo temperature in the right plot are as those of Fig. 5 plus 7×10^7, 10^8 K

the laboratory frame. Thus, for large positive halo velocity the kinetic energy of the dark atoms in the laboratory frame is small and, to have recoils with sufficient energy to fit the DAMA signal, large value of $\sqrt{f}\epsilon$ parameter are favoured. On the contrary, when the velocity of the halo is opposite to the Earth motion, the kinetic energy of the dark atoms in the laboratory increases and lower $\sqrt{f}\epsilon$ values are favoured. In hot scenario, the velocity of the dark atoms in the halo is high and it becomes the dominant contribution to the velocity of the particles in the laboratory frame. In this regime the allowed $\sqrt{f}\epsilon$ parameters converge to lower values for any halo velocity. When the velocity of the halo is high and opposite to the Earth, its contribution to the kinetic energy of the dark atoms in the laboratory frame is dominant with respect to the velocity distribution of the particles in the halo. In this case the allowed $\sqrt{f}\epsilon$ parameters is independent on the temperature of the halo. In the case of a pure Fe' halo there are no allowed region for negative halo velocity. In fact, the coupling of the Fe' mirror atoms with ordinary matter is high and the expected signal in case of a particle with high kinetic energy is too large to fit the DAMA observed annual modulation effect.

As discussed in the previous section we have considered many uncertainties regarding the models and the parameters needed in the calculation of the expected dark atoms signal. To show the impact of these uncertainties we have

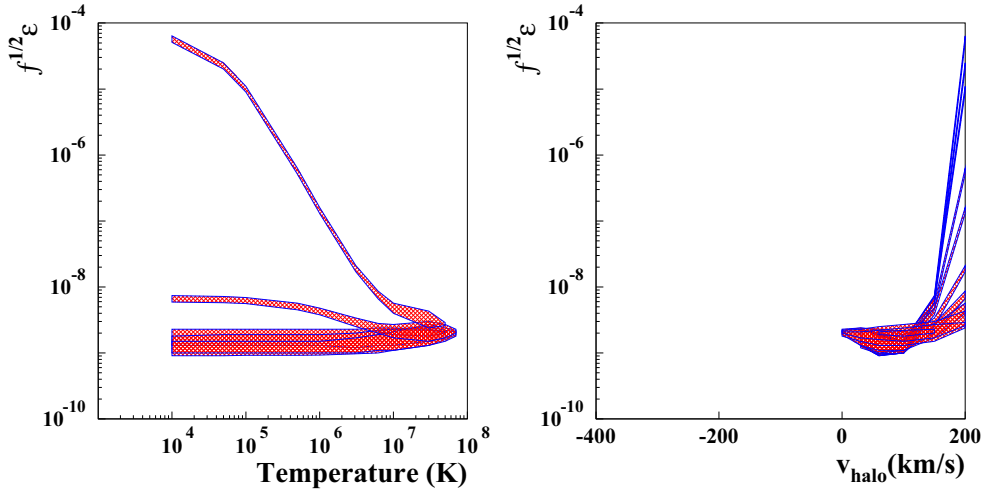

Fig. 9 Case of composite dark halo: H′(24%), He′(75%), Fe′(1%), in the scenario (*a*) of Table 3 with $v_0 = 220$ km/s and parameters in the set A (see text and Fig. 5). The different values of the halo velocity in the left plot are: 0, 30, 60, 100, 150, 200 km/s. The different values of the halo temperature in the right plot are as those of Fig. 5 plus 7×10^7 K

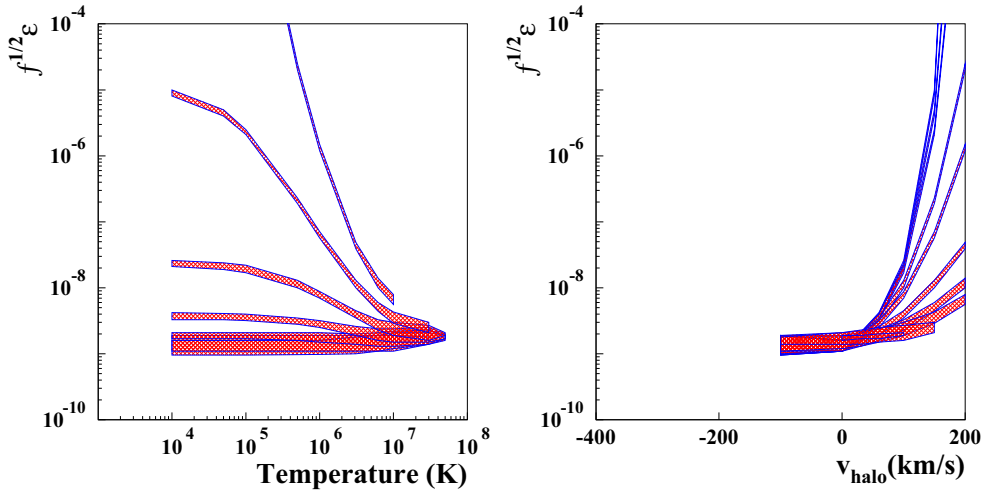

Fig. 10 Case of composite dark halo: H′(12.5%), He′(75%), C′(7%), O′(5.5%), in the scenario (*a*) of Table 3 with $v_0 = 220$ km/s and parameters in the set A (see text and Fig. 5). The different values of the halo velocity in the *left plot* are: −100, 0, 30, 60, 100, 150, 200 km/s. The different values of the halo temperature in the *right plot* are as those of Fig. 5

reported in the following the different allowed regions obtained for the same dark halo when different parameters and scenarios are considered. All the figures will have three plots corresponding to the following composite dark halo: (i) H′(12.5%), He′(75%), C′(7%), O′(5.5%) (left plot); (ii) H′(20%), He′(74%), C′(0.9%), O′(5%), Fe′(0.1%) (central plot); (iii) H′(24%), He′(75%), Fe′(1%) (right plot). These plots show the impact of the considered model framework and parameters to the $\sqrt{f}\epsilon$ allowed values.

In Fig. 12 the impact of the different adopted quenching factor is reported. The figures in the top (bottom) have been obtained by considering a halo temperature of 5×10^5 K (10^7 K); in each plots, the five scenarios of Table 3 have been considered for the three different halo models and different model frameworks. As it can be noted the allowed $\sqrt{f}\epsilon$ region can span over orders of magnitudes depending on the considered scenario.

In Fig. 13 allowed regions for the $\sqrt{f}\epsilon$ parameter as function of the halo temperature are reported to show the impact of the different scenarios of Table 3. The three panels refer to three different halo models and model framework.

In the Fig. 14 the allowed regions for the $\sqrt{f}\epsilon$ parameter as a function of the halo velocity for the three different v_0 values: 170, 220 and 270 km/s, are reported. The different

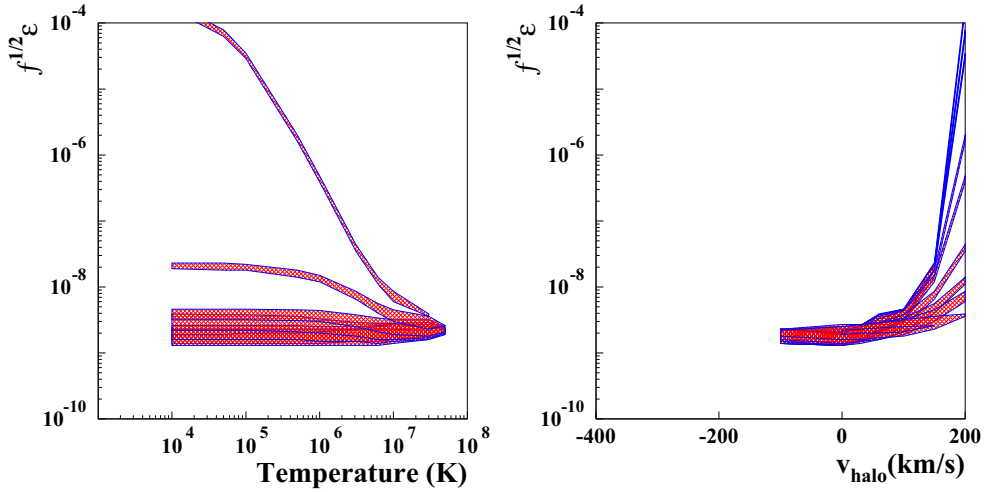

Fig. 11 Case of composite dark halo: H′(20%), He′(74%), C′(0.9%), O′(5%), Fe′(0.1%), in the scenario (*a*) of Table 3 with $v_0 = 220$ km/s and parameters in the set A (see text and Fig. 5). The different values of the halo velocity in the *left plot* are: −100, 0, 30, 60, 100, 150, 200 km/s. The different values of the halo temperature in the *right plot* are as those of Fig. 5

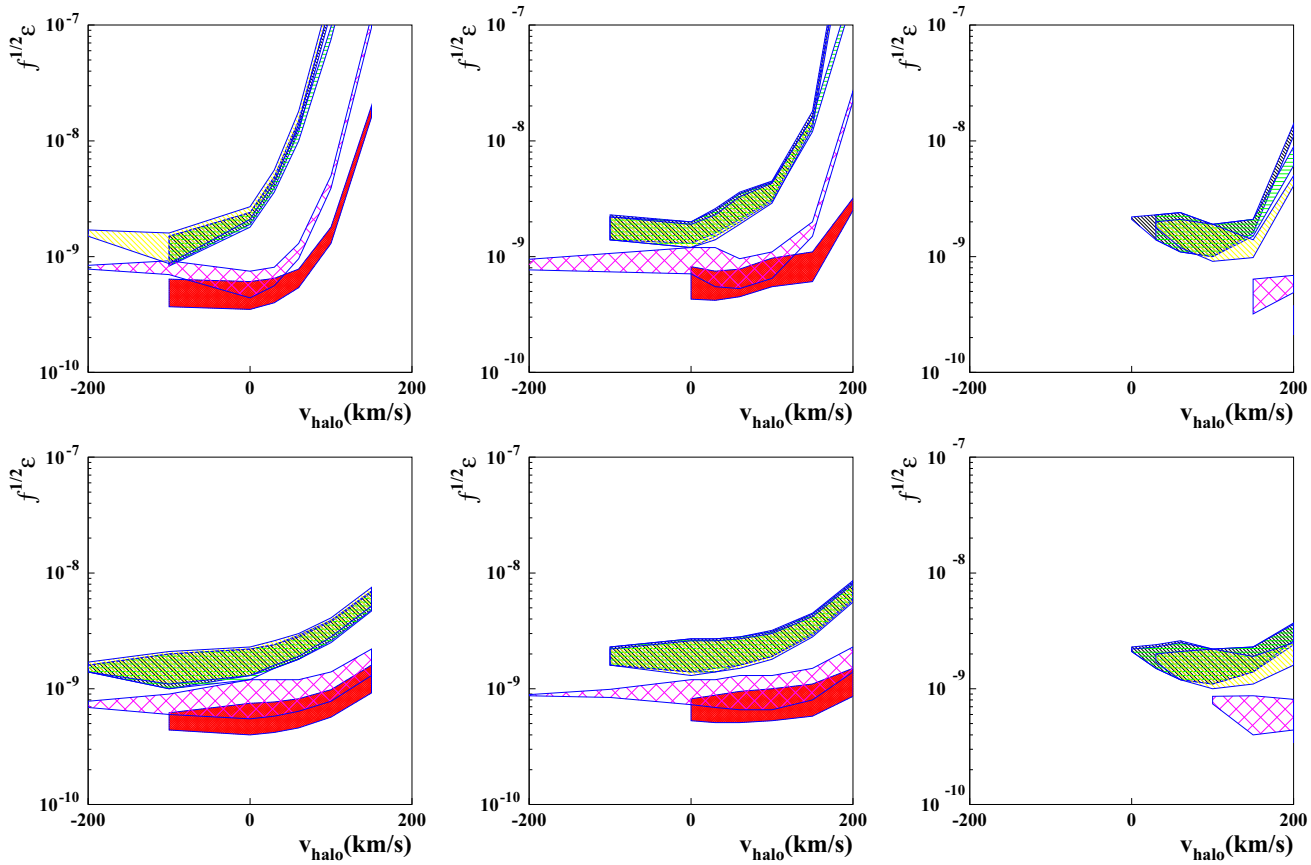

Fig. 12 Allowed regions for the $\sqrt{f}\epsilon$ parameter as a function of v_{halo}. The three graphs in the *top* (*bottom*) have been obtained by considering a halo temperature $T = 5 \times 10^5$ K ($T = 10^7$ K). The results of three different dark halo compositions and frameworks have been reported. *Left* Composite dark halo H′(12.5%), He′(75%), C′(7%), O′(5.5%), with $v_0 = 170$ km/s and parameters in the set B. *Center* Composite dark halo H′(20%), He′(74%), C′(0.9%), O′(5%), Fe′(0.1%), with $v_0 = 220$ km/s and parameters in the set A. *Right* Composite dark halo H′(24%), He′(75%), Fe′(1%), with $v_0 = 270$ km/s and parameters in the set C. Each graph has five contours corresponding to the scenarios of Table 3: from *bottom to top* the regions (see for example at $v_{halo} = 150$ km/s) refer to the cases (b), (d), (c), (a), (e), respectively

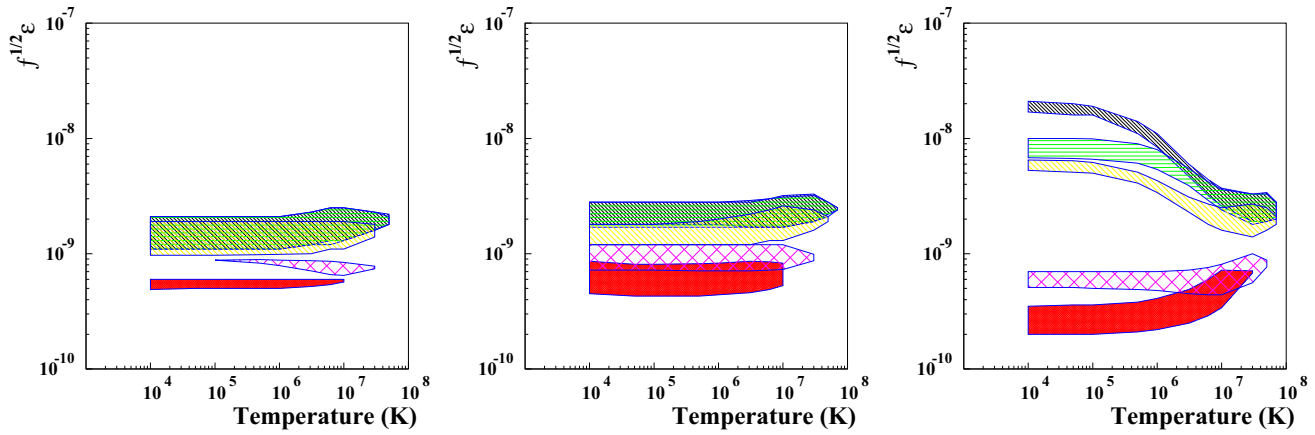

Fig. 13 Allowed regions for the $\sqrt{f}\epsilon$ parameter as function of the halo temperature. The three graphs refer to different dark halo composition and allow to compare the results obtained by considering the different scenarios of Table 3. The five contours in each plot correspond, from the *bottom to the top*, to the cases (b), (d), (c), (a), (e), respectively. *Left* Composite dark halo H′(12.5%), He′(75%), C′(7%), O′(5.5%), with $v_0 = 220$ km/s, $v_{halo} = -100$ km/s and parameters in the set C. *Center* Composite dark halo H′(20%), He′(74%), C′(0.9%), O′(5%), Fe′(0.1%), with $v_0 = 220$ km/s, $v_{halo} = 0$ km/s and parameters in the set C. *Right* Composite dark halo H′(24%), He′(75%), Fe′(1%), with $v_0 = 220$ km/s, $v_{halo} = 150$ km/s and parameters in the set C

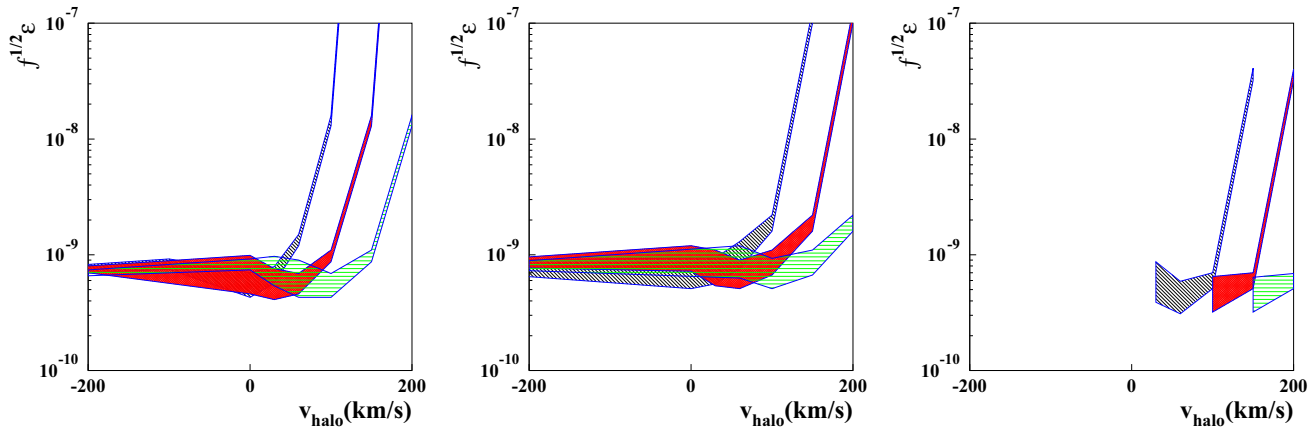

Fig. 14 Allowed regions for the $\sqrt{f}\epsilon$ parameter as function of v_{halo}. The three graphs refer to different dark halo compositions with the same temperature $T = 10^4$ K, the same set A and the same scenario (d): *Left* Composite dark halo H′(12.5%), He′(75%), C′(7%), O′(5.5%). *Center* Composite dark halo H′(20%), He′(74%), C′(0.9%), O′(5%), Fe′(0.1%). *Right* Composite dark halo H′(24%), He′(75%), Fe′(1%). The three contours in each plot correspond to $v_0 = 170$ km/s (area with *diagonal lines*) (*gray area on-line*), $v_0 = 220$ km/s (*shaded area*) (*red area on-line*), $v_0 = 270$ km/s (area with *horizontal lines*) (*green area on-line*), respectively

plots in this figure refer to different dark halo compositions with the same temperature $T = 10^4$ K, the same set A and the same scenario (d). From this figure it is possible to see the impact of the v_0 parameter in the evaluation of the allowed regions. Figure 15 shows the allowed regions for the $\sqrt{f}\epsilon$ parameter as a function of the halo temperature for the three different v_0 values by considering different dark halo.

It is worth noting that the v_0 parameter in the considered range of variability has impact on the allowed regions for low temperature halo when the halo velocity is positive and larger than 100 km/s.

Finally, to point out the impact of the uncertainties in the values of some nuclear parameters, represented by set A, B, and C, described above, in Fig. 16 the allowed regions for the $\sqrt{f}\epsilon$ parameter as a function of the halo velocity in the Galactic frame are reported for three different dark halo with the same temperature $T = 10^4$ K and $v_0 = 220$ km/s. In each plot the three different allowed regions correspond to the set A, B and C.

In conclusion, Figs. 12, 13, 14, 15, 16 show that the allowed values of the $\sqrt{f}\epsilon$ parameter span over almost two orders of magnitude depending on the halo temperature and on the halo velocity; these two parameters have a great impact in the allowed regions. As it can be noted in Figs. 12 and 13 the allowed regions have a clear dependence on the chosen scenario for the response of the detector (as in Table 3); sce-

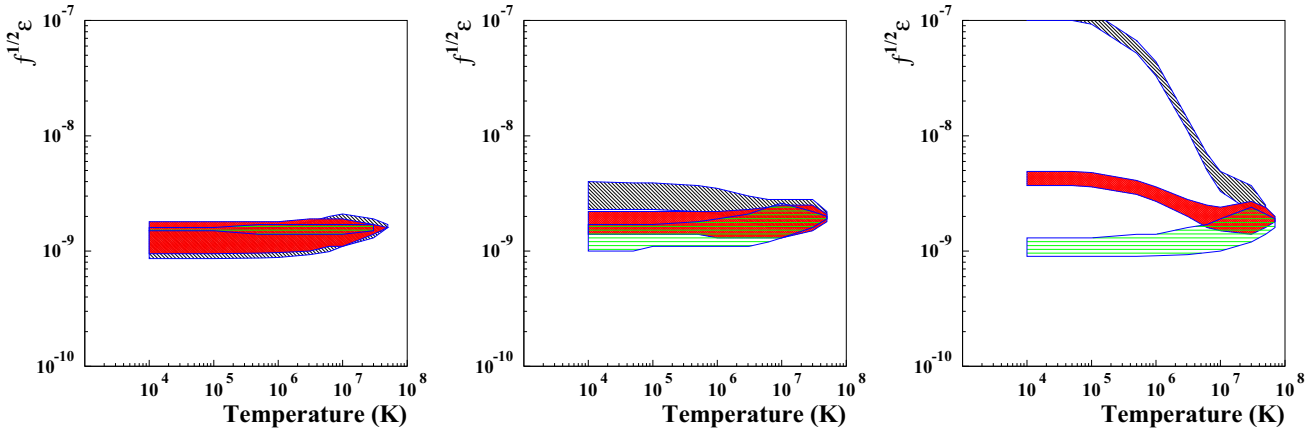

Fig. 15 Allowed regions for the $\sqrt{f}\epsilon$ parameter as function of the halo temperature. The three graphs refer to different dark halo composition and allow to compare the results obtained by considering different v_0: *Left* composite dark halo H′(12.5%), He′(75%), C′(7%), O′(5.5%), with $v_{halo} = -100$ km/s, scenario (e) and parameters in the set B. *Center* Composite dark halo H′(20%), He′(74%), C′(0.9%), O′(5%), Fe′(0.1%), with $v_{halo} = 30$ km/s, scenario (a) and parameters in the set B. *Right* Composite dark halo H′(24%), He′(75%), Fe′(1%), with $v_{halo} = 150$ km/s, scenario (c) and parameters in the set B. The three contours in each plot correspond to $v_0 = 170$ km/s (area with *diagonal lines*) (*gray area on-line*), $v_0 = 220$ km/s (*shaded area*) (*red area on-line*), $v_0 = 270$ km/s (area with *horizontal lines*) (*green area on-line*), respectively

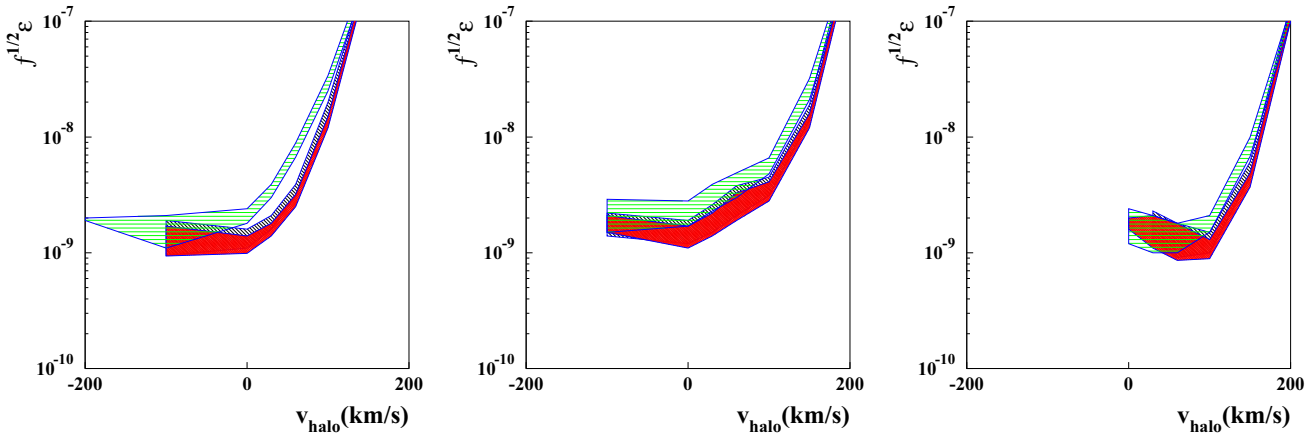

Fig. 16 Allowed regions for the $\sqrt{f}\epsilon$ parameter as function of v_{halo}. The three graphs refer to different dark halo compositions in the same scenario (c), the same temperature $T = 10^4$ K and $v_0 = 220$ km/s: *Left* Composite dark halo H′(12.5%), He′(75%), C′(7%), O′(5.5%). *Center* Composite dark halo H′(20%), He′(74%), C′(0.9%), O′(5%), Fe′(0.1%). *Right* Composite dark halo H′(24%), He′(75%), Fe′(1%). The three contours in each plot correspond to: set C (area with *horizontal lines*) (*green area on-line*), set A (area with *diagonal lines*) (*gray area on-line*), set B (*shaded area*) (*red area on-line*), respectively. The results obtained by considering the different sets of the parameters can be compared

narios with a better response at low energy, such e.g. the scenario (b), favour smaller values of $\sqrt{f}\epsilon$. The uncertainties on the Galactic local velocity, once the halo temperature is fixed, play a role only for positive halo velocities larger than about 100 km/s (see for example Fig. 14). The uncertainties on the parameters used in the nuclear form factors (the three different set A, B and C) have smaller impacts on the allowed regions. Finally, it is worth noting that many configurations exist that are well compatible with cosmological bounds. Obviously, introduction of other uncertainties and modelling is expected to further enlarge the allowed regions.

6 Conclusions

The mirror matter model has been considered to analyze the DM model-independent annual modulation effect observed by the DAMA Collaboration with NaI(Tl) target detectors. In the analysis we have assumed that a fraction f of the DM halo in the Galaxy is composed by mirror atoms of various species and we have derived allowed physical intervals for the parameters $\sqrt{f}\epsilon$, in various halo models. We have also accounted for some of the possible existing uncertainties. The results demonstrate that many configurations and halo

models favoured by the annual modulation effect observed by DAMA corresponds to $\sqrt{f}\epsilon$ values well compatible with cosmological bounds.

Finally it is worth noting that our analysis predict in most halo models an increase of the DM Mirror signal below 2 keV. These behaviours can be tested with the present DAMA/LIBRA phase2 that now is running.

Acknowledgements The authors gratefully acknowledge the whole DAMA Collaboration for the work which has produced the experimental results discussed here in particular framework of mirror Dark Matter. The work of A.A. and Z.B. was partially supported by the MIUR research grant "Theoretical Astroparticle Physics" PRIN 2012CPPYP7. The work of P.V. was supported by the MINECO grant "Ayudas a la movilidad predoctoral para la realización de estancias breves en centros I+D 2014", EEBB-I-15-10012.

References

1. A.K. Drukier, K. Freese, D.N. Spergel, Phys. Rev. D **33**, 3495 (1986)
2. K. Freese, J.A. Frieman, A. Gould, Phys. Rev. D **37**, 3388 (1988)
3. P. Belli, R. Bernabei, C. Bacci, A. Incicchitti, R. Marcovaldi, D. Prosperi, DAMA proposal to INFN Scientific Committee II, 24th April (1990)
4. R. Bernabei et al., Phys. Lett. B **389**, 757 (1996)
5. R. Bernabei et al., Phys. Lett. B **424**, 195 (1998)
6. R. Bernabei et al., Phys. Lett. B **450**, 448 (1999)
7. P. Belli et al., Phys. Rev. D **61**, 023512 (2000)
8. R. Bernabei et al., Phys. Lett. B **480**, 23 (2000)
9. R. Bernabei et al., Phys. Lett. B **509**, 197 (2001)
10. R. Bernabei et al., Eur. Phys. J. C **23**, 61 (2002)
11. P. Belli et al., Phys. Rev. D **66**, 043503 (2002)
12. R. Bernabei et al., Il Nuovo Cim. A **112**, 545 (1999)
13. R. Bernabei et al., Eur. Phys. J. C **18**, 283 (2000)
14. R. Bernabei el al., La Rivista del Nuovo Cimento **26**(1), 1–73 (2003)
15. R. Bernabei et al., Int. J. Mod. Phys. D **13**, 2127 (2004)
16. R. Bernabei et al., Int. J. Mod. Phys. A **21**, 1445 (2006)
17. R. Bernabei et al., Eur. Phys. J. C **47**, 263 (2006)
18. R. Bernabei et al., Int. J. Mod. Phys. A **22**, 3155 (2007)
19. R. Bernabei et al., Eur. Phys. J. C **53**, 205 (2008)
20. R. Bernabei et al., Phys. Rev. D **77**, 023506 (2008)
21. R. Bernabei et al., Mod. Phys. Lett. A **23**, 2125 (2008)
22. R. Bernabei et al., Phys. Lett. B **408**, 439 (1997)
23. P. Belli et al., Phys. Lett. B **460**, 236 (1999)
24. R. Bernabei et al., Phys. Rev. Lett. **83**, 4918 (1999)
25. P. Belli et al., Phys. Rev. C **60**, 065501 (1999)
26. R. Bernabei et al., Il Nuovo Cimento A **112**, 1541 (1999)
27. R. Bernabei et al., Phys. Lett. B **515**, 6 (2001)
28. F. Cappella et al., Eur. Phys. J.-Direct C **14**, 1 (2002)
29. R. Bernabei et al., Eur. Phys. J. A **23**, 7 (2005)
30. R. Bernabei et al., Eur. Phys. J. A **24**, 51 (2005)
31. R. Bernabei et al., Astropart. Phys. **4**, 45 (1995)
32. R. Bernabei, in the volume *The Identification of Dark Matter* (World Scientific Publishing, Singapore, 1997), p. 574
33. R. Bernabei et al., Nucl. Instr. Methods A **592**, 297 (2008)
34. R. Bernabei et al., Eur. Phys. J. C **56**, 333 (2008)
35. R. Bernabei et al., Eur. Phys. J. C **67**, 39 (2010)
36. R. Bernabei et al., Eur. Phys. J. C **73**, 2648 (2013)
37. P. Belli et al., Phys. Rev. D **84**, 055014 (2011)
38. R. Bernabei et al., J. Instr. **7**, P03009 (2012)
39. R. Bernabei et al., Eur. Phys. J. C **72**, 2064 (2012)
40. R. Bernabei et al., Int. J. Mod. Phys. A **28**, 1330022 (2013)
41. R. Bernabei et al., Eur. Phys. J. C **62**, 327 (2009)
42. R. Bernabei et al., Eur. Phys. J. C **72**, 1920 (2012)
43. R. Bernabei et al., Eur. Phys. J. A **49**, 64 (2013)
44. R. Bernabei et al., Eur. Phys. J. C **74**, 2827 (2014)
45. R. Bernabei et al., Eur. Phys. J. C **74**, 3196 (2014)
46. R. Bernabei et al., Eur. Phys. J. C **75**, 239 (2015)
47. A. Addazi et al., Eur. Phys. J. C **75**(8), 400 (2015). arXiv:1507.04317 [hep-ex]
48. T.D. Lee, C.N. Yang, Phys. Rev. **104**, 254 (1956)
49. I.Yu. Kobzarev, L.B. Okun, I.Ya. Pomeranchuk, Sov. J. Nucl. Phys. **3**, 837 (1966)
50. S.I. Blinnikov, M. Khlopov, Sov. Astron. **27**, 371 (1983)
51. S.I. Blinnikov, M. Khlopov, Astron. Zh. **60**, 632 (1983)
52. R. Foot, H. Lew, R.R. Volkas, Phys. Lett. B **272**, 67 (1991)
53. M.Y. Khlopov et al., Sov. Astron. **35**, 21 (1991)
54. M.Y. Khlopov et al., Astron. Zh. **68**, 42 (1991)
55. H.M. Hodges, Phys. Rev. D **47**, 456 (1993)
56. Z.G. Berezhiani, A.D. Dolgov, R.N. Mohapatra, Phys. Lett. B **375**, 26 (1996). arXiv:hep-ph/9511221
57. Z.G. Berezhiani, Acta Phys. Polon. B **27**, 1503 (1996). arXiv:hep-ph/9602326
58. R.N. Mohapatra, V.L. Teplitz, Astrophys. J. **478**, 29 (1997)
59. E.K. Akhmedov, Z.G. Berezhiani, G. Senjanovic, Phys. Rev. Lett. **69**, 3013 (1992). arXiv:hep-ph/9205230
60. Z.G. Berezhiani, R.N. Mohapatra, Phys. Rev. D **52**, 6607 (1995). arXiv:hep-ph/9505385
61. Z. Berezhiani, L. Gianfagna, M. Giannotti, Phys. Lett. B **500**, 286 (2001). arXiv:hep-ph/0009290
62. Z. Berezhiani, A. Drago, Phys. Lett. B **473**, 281 (2000). arXiv:hep-ph/9911333
63. Z. Berezhiani, D. Comelli, F.L. Villante, Phys. Lett. B **503**, 362 (2001). arXiv:hep-ph/0008105
64. A.Y. Ignatiev, R.R. Volkas, Phys. Rev. D **68**, 023518 (2003). arXiv:hep-ph/0304260
65. Z. Berezhiani, Int. J. Mod. Phys. A **19**, 3775 (2004). arXiv:hep-ph/0312335
66. Z. Berezhiani, P. Ciarcelluti, D. Comelli, F.L. Villante, Int. J. Mod. Phys. D **14**, 107 (2005). arXiv:astro-ph/0312605
67. P. Ciarcelluti, Int. J. Mod. Phys. D **14**, 223 (2005). arXiv:astro-ph/0409633
68. Z. Berezhiani, Through the looking-glass: Alice's adventures in mirror world. In *From Fields to Strings: Circumnavigating Theoretical Physics*, vol. 3, ed. by M. Shifman et al., pp. 2147–2195. arXiv:hep-ph/0508233
69. Z. Berezhiani, Eur. Phys. J. ST **163**, 271 (2008)
70. Z. Berezhiani, S. Cassisi, P. Ciarcelluti, A. Pietrinferni, Astropart. Phys. **24**, 495 (2006). arXiv:astro-ph/0507153
71. L. Bento, Z. Berezhiani, Phys. Rev. Lett. **87**, 231304 (2001). arXiv:hep-ph/0107281
72. L. Bento, Z. Berezhiani, Fortschr. Phys. **50**, 489 (2002)
73. L. Bento, Z. Berezhiani, Symposium on 100 Years Werner Heisenberg: Works and Impact, ed. by D. Papenfuss et al., arXiv:hep-ph/0111116
74. Z. Berezhiani, L. Bento, Phys. Rev. Lett. **96**, 081801 (2006). arXiv:hep-ph/0507031
75. B. Holdom, Phys. Lett. B **166**, 196 (1986)

76. S.L. Glashow, Phys. Lett. B **167**, 35 (1986)
77. S.N. Gninenko, Phys. Lett. B **326**, 317 (1994)
78. Z. Berezhiani, Phys. Lett. B **417**, 287 (1998). arXiv:hep-ph/9609342
79. A. Addazi, Z. Berezhiani, Y. Kamyshkov, Eur. Phys. J. C (in press). arXiv:1607.00348 [hep-ph]
80. R. Foot, R.R. Volkas, Phys. Rev. D **52**, 6595 (1995). arXiv:hep-ph/9505359
81. R.N. Mohapatra, S. Nasri, S. Nussinov, Phys. Lett. B **627**, 124 (2005). arXiv:hep-ph/0508109
82. Z. Berezhiani, L. Bento, Phys. Lett. B **635**, 253 (2006). arXiv:hep-ph/0602227
83. Z. Berezhiani, A. Gazizov, Eur. Phys. J. C **72**, 2111 (2012). arXiv:1109.3725 [astro-ph.HE]
84. Z. Berezhiani, Eur. Phys. J. C **64**, 421 (2009). arXiv:0804.2088 [hep-ph]
85. Z. Berezhiani, F. Nesti, Eur. Phys. J. C **72**, 1974 (2012). arXiv:1203.1035 [hep-ph]
86. Z. Berezhiani, arXiv:1602.08599 [astro-ph.CO]
87. R. Foot, Phys. Rev. D **69**, 036001 (2004). arXiv:hep-ph/0308254
88. R. Foot, Phys. Rev. D **88**(2), 025032 (2013). arXiv:1209.5602 [hep-ph]
89. Z. Berezhiani, AIP Conf. Proc. **878**, 195 (2006). arXiv:hep-ph/0612371
90. J. Bovy, H.W. Rix, Astrophys. J. **779**, 115 (2013)
91. Z. Berezhiani, D. Comelli, F. Nesti, L. Pilo, Phys. Rev. Lett. **99**, 131101 (2007). arXiv:hep-th/0703264 [HEP-TH]
92. Z. Berezhiani, L. Pilo, N. Rossi, Eur. Phys. J. C **70**, 305 (2010). arXiv:0902.0146 [astro-ph.CO]
93. Z. Berezhiani, F. Nesti, L. Pilo, N. Rossi, JHEP **0907**, 083 (2009). arXiv:0902.0144 [hep-th]
94. B.P. Abbott et al. [LIGO Scientific and Virgo Collaborations], Phys. Rev. Lett. **116**(6), 061102 (2016). arXiv:1602.03837 [gr-qc]
95. B.P. Abbott et al. [LIGO Scientific and Virgo Collaborations], Phys. Rev. Lett. **116**(24), 241103 (2016). arXiv:1606.04855 [gr-qc]
96. R. Schoenrich, J. Binney, W. Dehnen, MNRAS **403**, 1829–1833 (2010)
97. J. Delhaye in *Stars and Stellar Systems*, vol. 5 (University of Chicago Press, Chicago, 1965), p. 73
98. P. McMillan, J. Binney, MNRAS **402**, 934–940 (2010)
99. P.J.T. Leonard, S. Tremaine, Astrophys. J. **353**, 48 (1990)
100. C.S. Kochanek, Astrophys. J. **457**, 228 (1996)
101. K.M. Cudworth, Astron. J. **99**, 590 (1990)
102. M.J. Currie, D.S. Berry, T. Jenness et al. Starlink Software in 2013. Astronomical Data Analysis Software and Systems XXIII, **485**, 391 (2014). http://starlink.eao.hawaii.edu/starlink
103. A. Badertscher et al., Phys. Rev. D **75**, 032004 (2007). arXiv:hep-ex/0609059
104. E.D. Carlson, S.L. Glashow, Phys. Lett. B **193**, 168 (1987)
105. Z. Berezhiani, A. Lepidi, Phys. Lett. B **681**, 276 (2009). arXiv:0810.1317 [hep-ph]
106. Z. Berezhiani, S. Karshenboim, A. Kobakhidze, in preparation
107. Z. Berezhiani, A.D. Dolgov, I.I. Tkachev, Eur. Phys. J. C **73**, 2620 (2013). arXiv:1307.6953 [astro-ph.CO]
108. R.H. Helm, Phys. Rev. **104**, 1466 (1956)
109. J.D. Lewin, P.F. Smith, Astropart. Phys. **6**, 87 (1996)
110. V.I. Tretyak, Astropart. Phys. **33**, 40 (2010)
111. J.I. Collar, Phys. Rev. C **88**, 035806 (2013)
112. S.I. Matyukhin, Tech. Phys. **53**, 1578 (2008)
113. N. Bozorgnia et al., J. Cosm. Astropart. Phys. **11**, 19 (2010)